Article

Cell

Neural Precursor-Derived Pleiotrophin Mediates Subventricular Zone Invasion by Glioma

Graphical Abstract

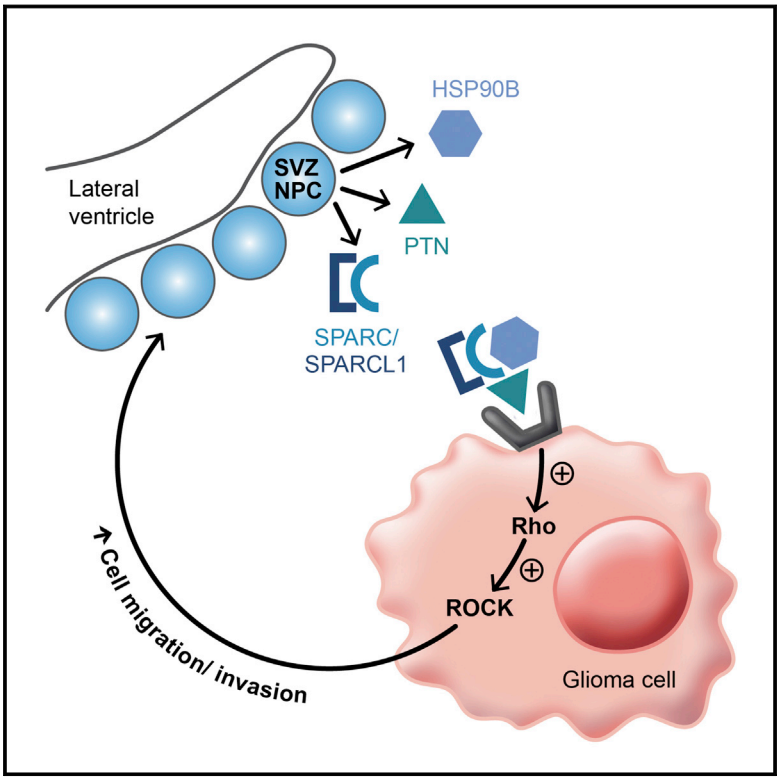

Authors

Elizabeth Y. Qin, Dominique D. Cooper, Keene L. Abbott, ..., Hannes Vogel, Peter K. Jackson, Michelle Monje

Correspondence

mmonje@stanford.edu

In Brief

The chemoattractant effect exerted by neural precursor cell-derived pleiotrophin underlies the preference of high-grade glioma to invade the lateral ventricle subventricular zone, providing potential targets for therapeutic development against glioma invasion.

Highlights

- Glioma invasion into the SVZ depends on signals from neural precursor cells (NPCs)
- Pleiotrophin (PTN) expression is highly enriched in the human and mouse SVZ
- NPCs secrete PTN, HSP90B, and SPARC/SPARCL1, which form a chemoattractant complex
- The PTN complex activates RhoA/ROCK signaling in glioma cells, promoting invasion

Qin et al., 2017, Cell *170*, 845–859
August 24, 2017
http://dx.doi.org/10.1016/j.cell.2017.07.016

CellPress

Cell

Neural Precursor-Derived Pleiotrophin Mediates Subventricular Zone Invasion by Glioma

Elizabeth Y. Qin,[1] Dominique D. Cooper,[1] Keene L. Abbott,[2] James Lennon,[1] Surya Nagaraja,[1] Alan Mackay,[4] Chris Jones,[4] Hannes Vogel,[1,3,5,6] Peter K. Jackson,[2,3] and Michelle Monje[1,3,5,6,7,*]
[1]Department of Neurology, Stanford University, Palo Alto, CA 94305, USA
[2]Baxter Laboratory, Department of Microbiology & Immunology, Stanford University, Palo Alto, CA 94305, USA
[3]Department of Pathology, Stanford University, Palo Alto, CA 94305, USA
[4]Divisions of Molecular Pathology and Cancer Therapeutics, The Institute of Cancer Research, London SM2 5NG, UK
[5]Department of Neurosurgery, Stanford University, Palo Alto, CA 94305, USA
[6]Department of Pediatrics, Stanford University, Palo Alto, CA 94305, USA
[7]Lead Contact
*Correspondence: mmonje@stanford.edu
http://dx.doi.org/10.1016/j.cell.2017.07.016

SUMMARY

The lateral ventricle subventricular zone (SVZ) is a frequent and consequential site of pediatric and adult glioma spread, but the cellular and molecular mechanisms mediating this are poorly understood. We demonstrate that neural precursor cell (NPC):glioma cell communication underpins this propensity of glioma to colonize the SVZ through secretion of chemoattractant signals toward which glioma cells home. Biochemical, proteomic, and functional analyses of SVZ NPC-secreted factors revealed the neurite outgrowth-promoting factor pleiotrophin, along with required binding partners SPARC/SPARCL1 and HSP90B, as key mediators of this chemoattractant effect. Pleiotrophin expression is strongly enriched in the SVZ, and pleiotrophin knock down starkly reduced glioma invasion of the SVZ in the murine brain. Pleiotrophin, in complex with the binding partners, activated glioma Rho/ROCK signaling, and ROCK inhibition decreased invasion toward SVZ NPC-secreted factors. These findings demonstrate a pathogenic role for NPC:glioma interactions and potential therapeutic targets to limit glioma invasion.

INTRODUCTION

High-grade gliomas (HGGs) are a diffusely infiltrating group of cancers with dire prognoses. The lateral ventricle subventricular zone (SVZ) stem cell niche is thought to be a tumor reservoir for a range of HGGs including adult glioblastoma (GBM). Glioma contact of neural stem cell niches, particularly the SVZ, has been closely associated with decreased survival (Chaichana et al., 2008; Jafri et al., 2013; Mistry et al., 2017a, 2017b) and increased tumor recurrence (Adeberg et al., 2014; Chen et al., 2015). Diffuse intrinsic pontine glioma (DIPG; recently re-classified as diffuse midline glioma, H3K27M mutant) (Louis et al., 2016) is the most common HGG of childhood and the leading cause of pediatric brain tumor-related death, with a median survival of only 9 months and a 5-year survival of <1% (Donaldson et al., 2006). DIPG tends to not only infiltrate the brainstem where it originates, but also spreads distantly to the lateral ventricle SVZ in ~65% of cases (Caretti et al., 2014). A point of debate regarding SVZ involvement in adult GBM has been whether gliomas spread to the SVZ or the cancer originates there. In DIPG, the tumor clearly begins in the pons and from some anatomical distance spreads to the SVZ, clarifying the propensity of HGGs to travel to the SVZ niche. DIPG is thus an illustrative tumor type in which to discern the mechanisms of SVZ invasion that may be broadly relevant to HGGs. In the present study, we sought to understand how and why DIPG and other HGGs spread so frequently to the SVZ, hypothesizing that this predilection could be mediated by interactions between the glioma cells and the neural precursor cells (NPCs) that normally reside in the SVZ (Sanai et al., 2004).

RESULTS

SVZ-Derived DIPG Cells Recapitulate Invasion Pattern in an Orthotopic Xenograft Model

We had the opportunity to culture DIPG at the time of early postmortem autopsy from tumor in the pons and tumor in the SVZ (cultures designated SU-DIPG-XIII pons and SU-DIPG-XIII frontal lobe, also referred to as SVZ DIPG cells; Figure 1A; please see Figures S1A–S1D for genomic and gene expression characterizations of both cultures). In this case, the pontine tumor had been treated with radiation therapy while the SVZ metastases were treatment-naive. While tumor spread to the lateral ventricle SVZ is frequent (Figures 1B, 1C, and S1E–S1H), a culture of DIPG cells from an SVZ site of spread has not previously been established and provides a rare and valuable resource. Pontine and SVZ DIPG cells were transduced to express GFP and luciferase and subsequently orthotopically xenografted into the pons of juvenile immunodeficient (NOD-SCID-IL2R γ-chain-deficient; NSG) mice. Bioluminescent imaging (IVIS) indicated that SVZ DIPG cells invaded supratentorially to the cerebrum (Figure 1D), while the pontine DIPG cells from

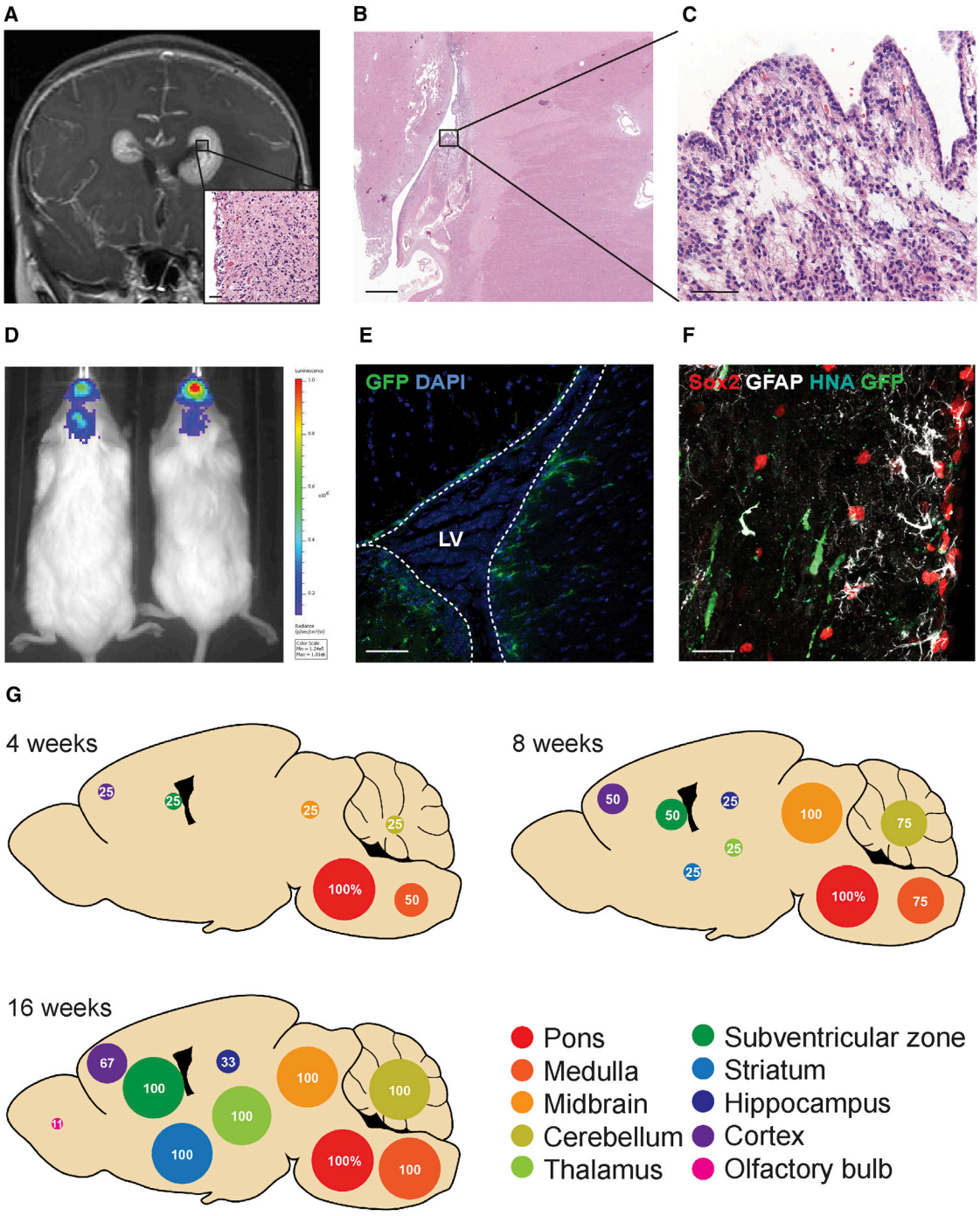

Figure 1. DIPG Cells Isolated from an SVZ Site of Spread Invade to the Cerebrum and SVZ

(A) MRI (coronal, T1 post-gadolinium) and H&E micrograph (inset) of tumor in the SVZ of a 6-year-old female with DIPG (subject SU-DIPG-XIII). Scale bar, 50 μm.

(B and C) H&E micrographs of tumor in the lateral wall of the lateral ventricle SVZ in a 12-year-old female with DIPG (subject SU-DIPG-V). Scale bars, 1 mm (B), 50 μm (C).

(D and E) DIPG cells isolated from tumor in the SVZ (SU-DIPG-XIII FL cells) recapitulate invasion of the forebrain when orthotopically xenografted in NSG mice as shown in bioluminescent IVIS imaging (D), as well as invasion of the SVZ as shown by histological analysis (E). Lateral ventricle outlined in dashed white lines. Scale bar, 40 μm.

(F) SU-DIPG-XIII FL cells (GFP^+ HNA^+) and neural precursor cells ($Sox2^+$ $GFAP^+$) in the SVZ stem cell niche in an NSG mouse orthotopically xenografted with DIPG cells. Scale bar, 20 μm.

(G) SU-DIPG-XIII FL cells invade widely throughout the brain over time, with 100% of mice exhibiting tumor in the SVZ by 16 weeks post-xenograft.

See also Figure S1.

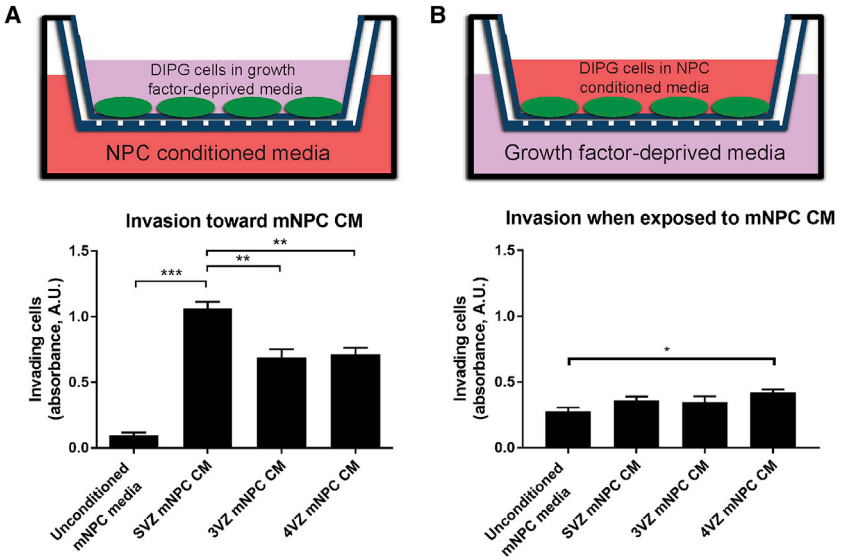

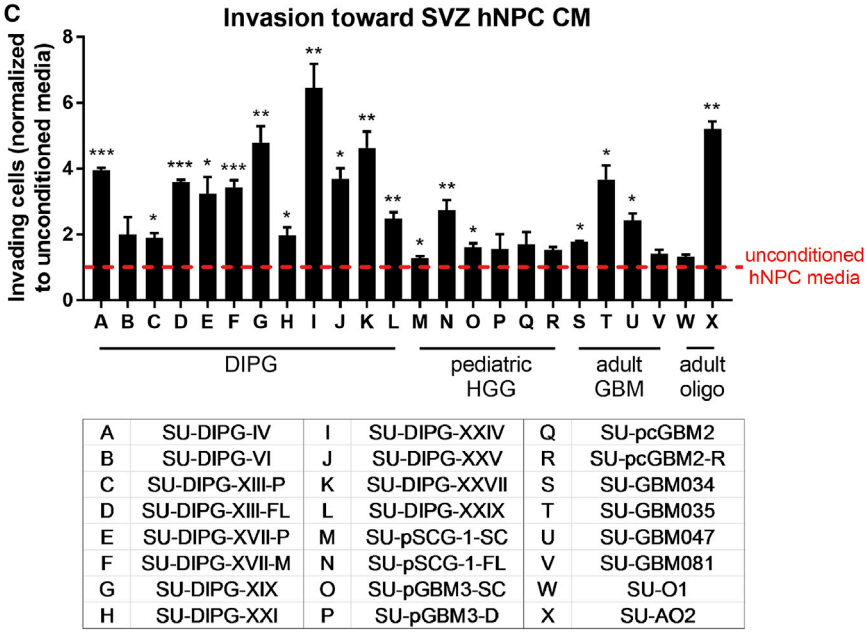

A	SU-DIPG-IV	I	SU-DIPG-XXIV	Q	SU-pcGBM2
B	SU-DIPG-VI	J	SU-DIPG-XXV	R	SU-pcGBM2-R
C	SU-DIPG-XIII-P	K	SU-DIPG-XXVII	S	SU-GBM034
D	SU-DIPG-XIII-FL	L	SU-DIPG-XXIX	T	SU-GBM035
E	SU-DIPG-XVII-P	M	SU-pSCG-1-SC	U	SU-GBM047
F	SU-DIPG-XVII-M	N	SU-pSCG-1-FL	V	SU-GBM081
G	SU-DIPG-XIX	O	SU-pGBM3-SC	W	SU-O1
H	SU-DIPG-XXI	P	SU-pGBM3-D	X	SU-AO2

Figure 2. Factors Secreted by NPCs Promote High-Grade Glioma Invasion

(A and B) Schematic and Matrigel invasion assay results of DIPG cells invading toward mNPC CM (A) or when co-incubated with mNPC CM (B). DIPG cells invade preferentially toward SVZ mNPC CM compared to other mNPC CM or unconditioned mNPC medium. Direct exposure to 4VZ mNPC CM modestly increases general DIPG invasion. n = 3 replicates/wells in SU-DIPG-XIII FL cells and analyzed by one-way ANOVA with Tukey post hoc adjustment for multiple comparisons.

(C) 18 out of a panel of 24 patient-derived glioma cultures (see Table S1) invade preferentially toward SVZ hNPC CM compared to unconditioned hNPC medium. n = 3 replicates/wells and analyzed by unpaired, two-tailed Student's t tests for comparison between unconditioned and conditioned hNPC medium.

Data shown as mean ± SEM. *$p < 0.05$, **$p < 0.01$, ***$p < 0.001$.

See also Figure S2 and Table S1.

Secreted Factors from NPCs Promote Glioma Invasion

To test the invasion of glioma toward NPCs in vitro, we utilized a Boyden chamber Matrigel invasion assay, which allows for chemoattraction testing and mimics invasion through an extracellular matrix. A suspension of SVZ DIPG cells placed on top of the Matrigel layer was allowed to invade toward medium conditioned by mouse NPCs (mNPC CM) isolated from the lateral ventricle subventricular zone (SVZ), third ventricular zone (3VZ), or fourth ventricular zone (4VZ), or toward unconditioned mNPC medium for 72 hr. In this paradigm, SVZ DIPG cells showed the strongest preferential invasion toward SVZ mNPC CM, with less robust preferential invasion toward 3VZ or 4VZ mNPC CM, compared to unconditioned mNPC medium (Figure 2A). When the paradigm was reversed (SVZ DIPG cells co-incubated with mNPC CM and allowed to invade toward growth factor-deprived medium), SVZ DIPG cells co-incubated with 4VZ mNPC CM showed a small increase in general invasion (Figure 2B). Exposure to medium conditioned by any of the mNPC populations did not affect DIPG cell proliferation or viability (Figures S2A and S2B). These data suggest that SVZ DIPG cells, which are intrinsically invasive, can modestly increase general invasiveness upon direct exposure to molecules secreted by 4VZ mNPCs and have strong preferential invasion toward chemoattractant molecules secreted by SVZ mNPCs. To assess the relative specificity of invasion toward NPCs and to control for the possible chemoattractant effects of molecules secreted by cells in general, we tested invasion toward factors secreted by cultured murine neurons and found only a minimal effect; SVZ

this case remained localized primarily to the hindbrain (Figure S1I). The ability of the SVZ DIPG cells to invade widely may be due to higher expression of genes involved in extracellular matrix degradation, including matrix metalloproteinases and ADAM metallopeptidases (Figures S1C and S1D). Histological analyses showed a diffusely infiltrating pattern of spread of SVZ DIPG cells that consistently demonstrated spread into the mouse SVZ (Figure 1E), with glioma cells in close proximity to the SVZ NPCs within the stem cell niche (Figure 1F). Spread of SVZ DIPG cells throughout the brain increased over time, with 100% of mice exhibiting widespread tumor and infiltration of the SVZ by 16 weeks post-xenograft (Figure 1G). This mouse model of SVZ invasion recapitulates the clinical behavior of the tumor and enables study of the mechanisms mediating invasion of the NPC niche.

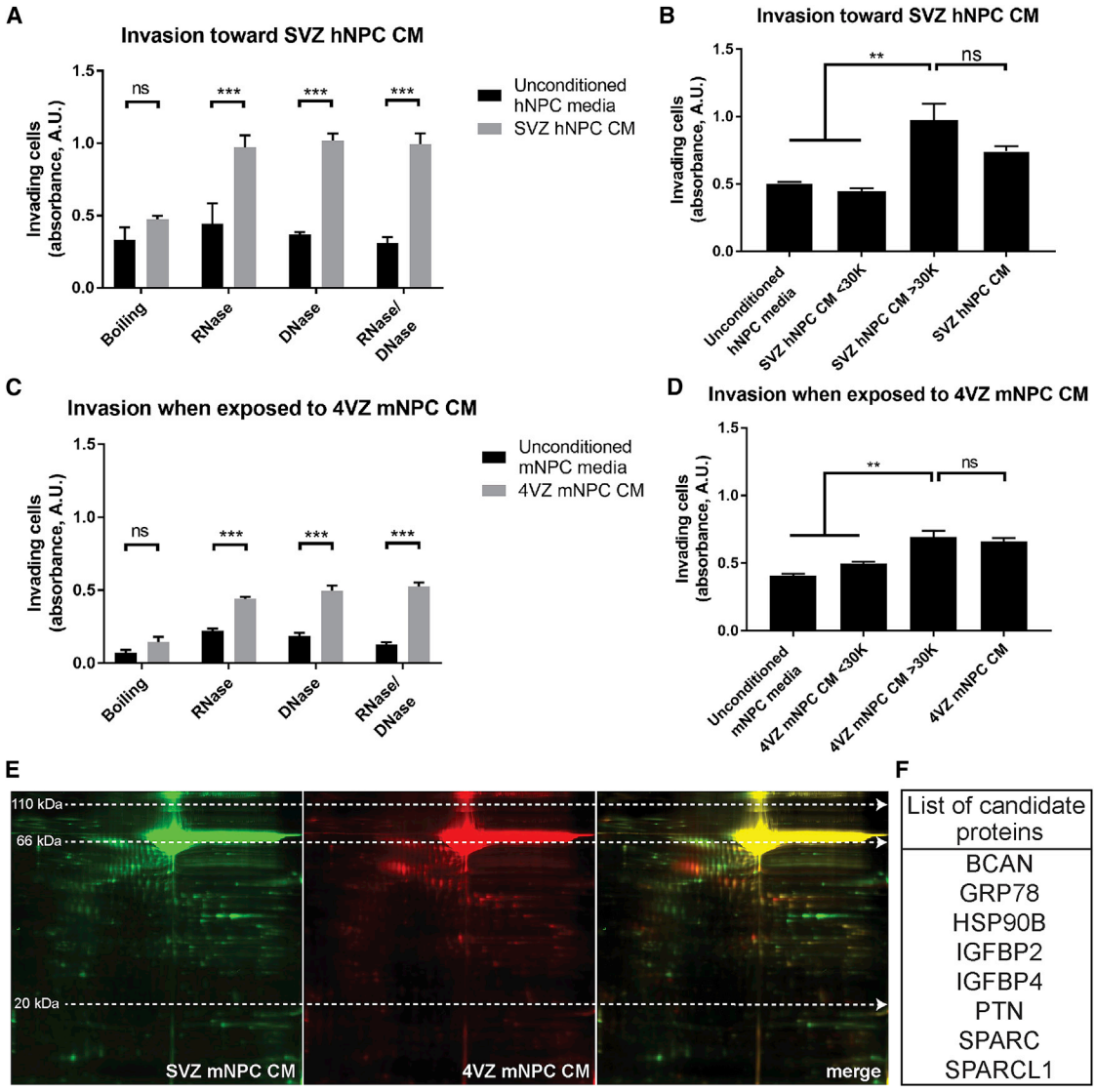

Figure 3. NPC-Secreted Factors Promoting Invasion Are Proteins

(A and C) Boiling, but not RNase and/or DNase treatment, abrogates the invasion-promoting effects of SVZ hNPC CM (A) and 4VZ mNPC CM (C).

(B and D) Size fractionation of SVZ hNPC CM (B) and 4VZ mNPC CM (D) reveals that the invasion-promoting factor(s) are >30 kDa in size. All experiments performed with n = 3 replicates/wells in SU-DIPG-XIII FL cells and analyzed by unpaired, two-tailed Student's t tests for comparison between unconditioned and conditioned medium (A and C) or by one-way ANOVA with Tukey post hoc adjustment for multiple comparisons (B and D). Data shown as mean ± SEM. $^{**}p < 0.01$, $^{***}p < 0.001$.

(E) Two-dimensional gel electrophoresis separating proteins in SVZ mNPC CM (green) and 4VZ mNPC CM (red) by size (vertical axis) and charge (horizontal axis).

(F) List of candidate proteins of interest identified from proteomic analysis that were differentially expressed in SVZ mNPC CM compared to 4VZ mNPC CM by a factor of 1.5.

mNPC CM promoted a substantially more robust increase in DIPG invasion compared to murine neuronal CM (Figure S2C). We next evaluated the CM from a culture of human fetal SVZ NPCs and found a similar chemoattractant effect on SVZ DIPG cells (Figure 2C). Expanding these observations, we found that 18 out of a panel of 24 patient-derived glioma cell cultures, including DIPG, pediatric spinal cord glioma, pediatric cortical GBM, adult GBM, and oligodendroglioma, demonstrated increased invasion toward human SVZ NPC CM compared to unconditioned human neural precursor cell (hNPC) medium (Figure 2C; Table S1). These results indicate that a range of molecularly distinct classes of HGGs exhibit preferential invasion toward factors secreted by SVZ NPCs.

NPC-Derived Secreted Factors Promoting Glioma Invasion Are Proteins

We performed several biochemical analyses to determine the nature of the NPC-secreted factors. Heat inactivation of SVZ hNPC CM abrogated its chemoattractant effect, whereas RNase and DNase treatment did not (Figure 3A). Size fractionation of the

CM showed that DIPG cells exhibited strong invasion toward the >30 kDa fraction, but not toward the <30 kDa fraction (Figure 3B). Together, these data indicate that the SVZ hNPC-secreted chemoattractant(s) are protein(s) >30 kDa in size. Similarly, the invasion-promoting factor(s) in the 4VZ mNPC CM also appear to be protein(s) >30 kDa (Figures 3C and 3D). To identify the invasion-promoting proteins present in SVZ and 4VZ mNPC CM, we utilized 2D gel electrophoresis to separate the secreted proteins by size and charge, followed by mass spectrometry to identify the differentially secreted protein spots (Figure 3E). Spots differentially detected in SVZ mNPC CM compared to 4VZ mNPC CM by a factor of 1.5 were selected for further investigation. These analyses generated a list of candidate proteins that were differentially secreted by SVZ and 4VZ mNPCs (Figure 3F).

Pleiotrophin, in Combination with Required Binding Partners, Promotes Glioma Invasion toward the SVZ

We subsequently tested the sufficiency of each of the eight candidate proteins to chemoattract DIPG cells. Using human recombinant proteins in the Matrigel invasion assay, we tested directed invasion of DIPG cells toward each candidate factor. No significant increase in invasion was observed for individual candidate proteins compared to unconditioned medium (Figure 4A). We then tested DIPG invasion toward various combinations of the candidate proteins and found the combination of four proteins: pleiotrophin (PTN), secreted protein acidic and rich in cysteine (SPARC), SPARC-like protein 1 (SPARCL1), and heat shock protein 90B (HSP90B), exhibits a chemoattractant effect most similar to that of the SVZ hNPC CM (Figure S3A). Testing combinations of two, three, or all four of these proteins demonstrated that only the combination of all four proteins was sufficient to recapitulate the full invasion-promoting effect of SVZ hNPC CM (Figure 4B). PTN is present in the highest concentration of the four proteins in SVZ hNPC CM as estimated by immunoblot (Figure S3B). The estimated concentrations of the four proteins in SVZ hNPC CM were confirmed to be sufficient for DIPG invasion (Figure S3C).

In order to elucidate the nature of the interaction between the four proteins, we performed biochemical analyses to determine the size and binding interactions of the proteins of interest in SVZ hNPC CM. By size exclusion chromatography of concentrated SVZ hNPC CM and subsequent immunoblot analysis of the eluted fractions, we found that the four proteins of interest all coeluted at approximately the size that would be expected for a complex of all four proteins (Figure 4C). With the exception of SPARCL1, the four proteins had similar patterns of elution and fractionated mostly at the larger size of all four proteins combined rather than at the sizes of the single proteins. This suggests that the proteins exist primarily as part of a four-protein complex. Furthermore, in immunoprecipitation (IP) reactions, we found that by immunoprecipitating any one of the four proteins, all four proteins copurified and did not precipitate with a control IgG antibody (Figure 4D). To assess the specificity of the IP pull-down assay, three control proteins also present in SVZ hNPC CM, 78 kDa glucose-regulated protein (GRP78), insulin-like growth factor binding protein 2 (IGFBP2), and brevican (BCAN), were immunoprecipitated and were not found to copurify with any of the four proteins (Figure 4D). These results further demonstrate that the four proteins physically interact and specifically bind together as a single complex. Of the four identified proteins, PTN was of particular interest, as it has been demonstrated to promote adult GBM cell migration through autocrine/paracrine action (Lu et al., 2005; Ulbricht et al., 2003). The requirement of SPARC, SPARCL1, and HSP90B as binding partners for PTN in promoting glioma invasion is consistent with the role of SPARC and SPARCL1 as adaptor proteins that act as connecting molecules (Lane and Sage, 1994) and the role of HSP90B as a chaperone protein facilitating the interactions of other proteins (Wiech et al., 1992). The binding of these three proteins may act to stabilize PTN, which has been shown to promote haptotactic glioma cell migration, i.e., migration toward immobilized PTN, as opposed to chemotactic migration toward free soluble PTN molecules (Lu et al., 2005; Ulbricht et al., 2003). Similar to the conserved invasive response toward SVZ hNPC CM, we found that 9 out of 9 patient-derived glioma cell cultures, including DIPG, pediatric spinal cord glioma, adult GBM, and anaplastic oligodendroglioma, invaded toward the combination of PTN and its three binding partners (Figure 4E). As an example of a cancer with known metastatic tropism for the brain, but that does not preferentially spread to the SVZ, we tested a melanoma cell line and found that it did not invade toward SVZ hNPC CM or toward the PTN complex (Figure S3D). Together, these results indicate that PTN and its three binding partners form a complex and signal as a unit in promoting the directional invasion of a range of HGGs.

Expression of Pleiotrophin Is Strongly Enriched in the Mouse and Human Postnatal SVZ

Pleiotrophin has been found to promote neurite outgrowth and neuroblast migration during neurodevelopment (Li et al., 1990; Rauvala and Pihlaskari, 1987; Maeda and Noda, 1998), as well as migration of adult GBM cells through autocrine/paracrine mechanisms (Lu et al., 2005; Ulbricht et al., 2003). We found that PTN protein expression is enriched in the SVZ stem cell niche compared to other brain regions, with PTN expression strongest in the lateral ventricle SVZ, particularly in the lateral walls, and moderate expression in the third and fourth ventricular zone in the adult murine brain (Figure 5A). In the developing postnatal murine brain, we found that PTN protein is more broadly expressed in the brain at P0–P5 and becomes largely restricted to the lateral ventricle SVZ by P10 (Figures 5B and S4A). PTN protein is also expressed in the pia mater, which is interesting to note as HGGs can also spread to the leptomeninges; in DIPG, leptomeningeal spread has been observed in 25%–30% of cases at the time of autopsy (Caretti et al., 2014) (Figures 5B and S4A). Of the four identified proteins, PTN is the most localized to the SVZ after early postnatal development in mice, whereas SPARC, SPARCL1, and HSP90B are more broadly expressed in the brain (Figure S4A). In the childhood and adult human SVZ, we found strong PTN expression specific to the first few millimeters subjacent to the ventricular epithelium and expression co-localized with Nestin$^+$ NPCs as well as extracellularly (Figures 5C and 5D). NPCs isolated from the murine lateral ventricle SVZ at P14 exhibit higher gene and protein expression of PTN compared to NPCs isolated at the same age from the 3VZ, 4VZ, or hippocampal dentate gyrus (another neural stem cell niche; Figures 5E and 5G). Whole SVZ tissue isolated from

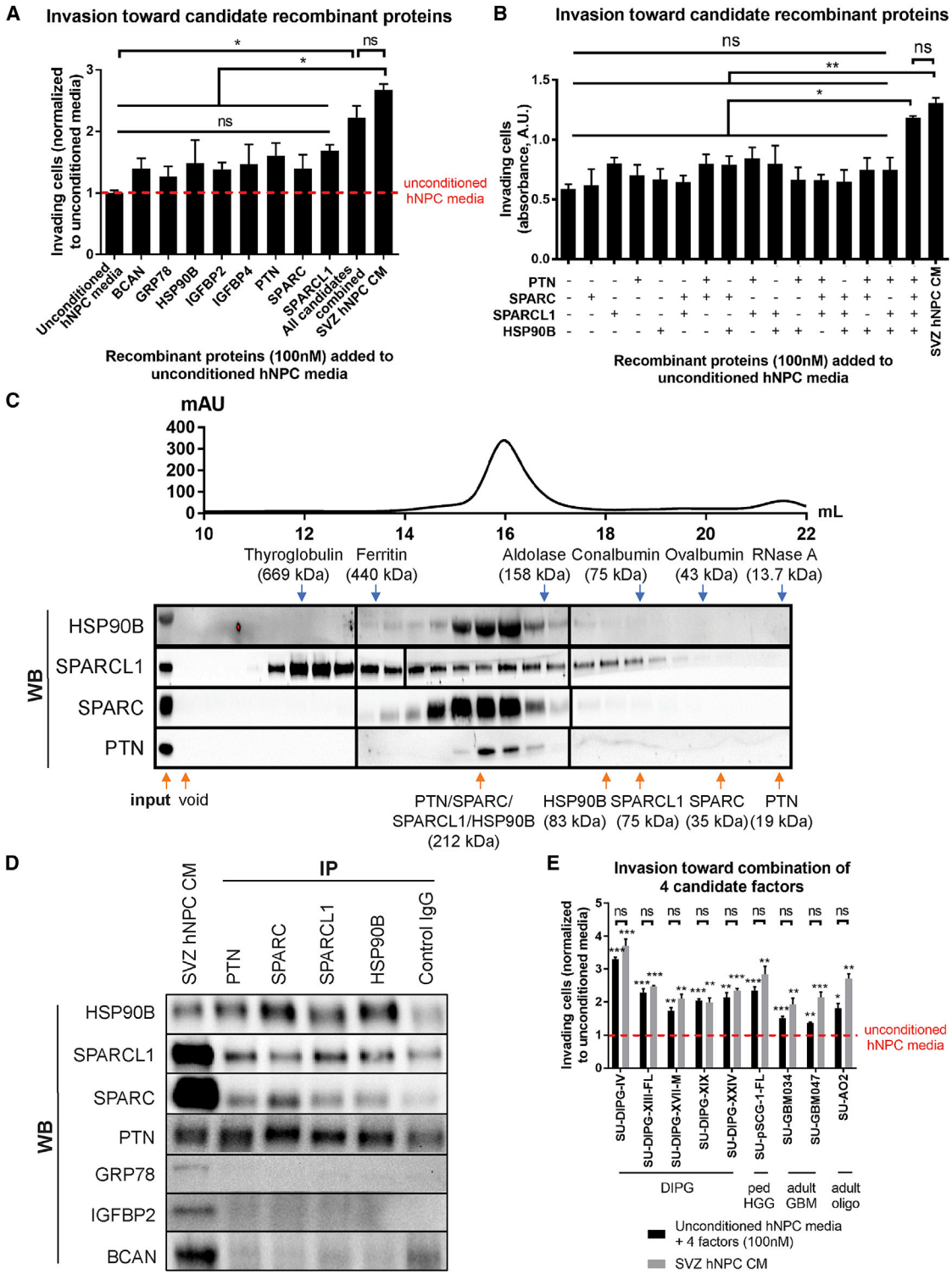

Figure 4. The Combination of PTN and Three Required Binding Partners Promotes DIPG Invasion toward SVZ hNPC CM

(A) No single candidate recombinant protein significantly increased DIPG invasion compared to unconditioned hNPC medium.

(B) The combination of four factors: PTN, SPARC, SPARCL1, and HSP90B, was sufficient for the full invasion-promoting effect toward SVZ hNPC CM. No combination of two or three factors was sufficient. All experiments performed with n = 3 replicates/wells in SU-DIPG-XIII FL cells and analyzed by one-way ANOVA with Tukey post hoc adjustment for multiple comparisons (A) or Dunnett post hoc adjustment for multiple comparisons to either SVZ hNPC CM or the combination of all 4 factors (B).

(legend continued on next page)

P42 mice also exhibits higher gene and protein expression of PTN compared to cortical tissue (Figures 5F and 5H). These results demonstrate the specific enrichment of PTN in murine and human postnatal SVZ NPCs, suggesting that this molecule could mediate NPC:glioma chemoattraction and underlie the pattern of SVZ invasion observed clinically. Together, these results suggest that PTN is a primary factor responsible for the chemoattraction toward SVZ hNPC CM, and the other three proteins act as accessory factors.

PTN Is Necessary for Glioma Invasion toward the SVZ

To test the necessity of the PTN complex for DIPG invasion toward SVZ NPCs, we depleted each factor from SVZ hNPC CM by two different methods. Immunodepletion of any of the four proteins (with or without add back of the other three proteins) abrogated the chemoattractant effect of the CM (Figures 6A and S5A). Small hairpin RNA (shRNA)-mediated knock down of SVZ hNPC gene expression of any of the four genes decreased DIPG cell invasion toward CM from those NPCs (Figure 6B). These results indicate that each of the four proteins is necessary for DIPG invasion toward SVZ NPCs in vitro. We then tested the necessity of PTN for DIPG invasion of the SVZ in vivo. Stereotactic injection of lentivirus expressing shRNA targeting *Ptn* into the mouse SVZ achieved effective knock down of pleiotrophin expression, compared to a non-targeting scrambled shRNA control (Figure 6C). Tumor engraftment in the two groups was equivalent (Figure S5B). At 16 weeks following pontine xenograft, we found that fewer DIPG cells invaded the SVZ in mice with shRNA-mediated knock down of *Ptn* in the SVZ, compared to mice that received a scrambled shRNA control (Figures 6C and 6E). While the role of PTN in postnatal SVZ NPCs remains to be elucidated, we assessed the number of SVZ NPCs present following *Ptn* knock down to confirm that the striking decrease in SVZ glioma invasion was not explained by a reduction in the NPC population. We found equivalent numbers of $Sox2^+$ NPCs in mice injected with *Ptn* shRNA or scrambled shRNA control vectors (Figures 6D and 6F), confirming that the observed reduction in glioma invasion was not due to NPC loss but rather to decreased *Ptn* expression. Taken together, these data demonstrate that PTN is necessary for glioma invasion toward the SVZ NPC niche in vitro and in vivo.

Pleiotrophin has several known receptors and the one that has been implicated in glioma migration is protein tyrosine phosphatase receptor type ζ (PTPRZ) (Lu et al., 2005; Müller et al., 2003; Ulbricht et al., 2003). DIPG primary tumor and cell culture samples exhibit expression of the protein tyrosine phosphatase receptor type ζ gene *PTPRZ1* (Grasso et al., 2015; Nagaraja et al., 2017) (Figure S5C). Robust shRNA-mediated knock down of *PTPRZ1* expression in DIPG cells (Figure S5D) substantially decreases baseline invasion (Figure S5E) and also mildly decreases cell viability (Figure S5F). Normalizing for these effects, we find that *PTPRZ1* knock down in DIPG cells confers a partial abrogation of invasion toward SVZ hNPC CM or the PTN complex in vitro (Figure S5G). This suggests that while PTPRZ is necessary for the full effect of the PTN complex, other receptors may also be involved. To further test the hypothesis that PTPRZ is a relevant PTN receptor to SVZ invasion, *PTPRZ1* knock down or scrambled control DIPG cells were xenografted to the pons. We found a dramatic effect on engraftment, with *PTPRZ1* knock down resulting in 10-fold lower bioluminescent signal on initial IVIS imaging (Figure S5H). From these different initial tumor sizes, the rate of growth was similar in mice xenografted with *PTPRZ1* knock down or control cells (Figure S5I). At 8 weeks, significantly fewer cells expressing *PTPRZ1* shRNA reached the SVZ (Figure S5J), but interpretation of these results is complicated by the substantial effect of *PTPRZ1* knock down on DIPG xenograft engraftment.

HSP90 Inhibition as a Potential Therapeutic Strategy

Because HSP90B is a necessary component of the PTN complex, and HSP90 inhibitors have been developed for clinical use, we tested the possibility that HSP90 inhibition could be used as a strategy to reduce SVZ invasion. Evaluating an HSP90 inhibitor (tanespimycin, 17-AAG) that has been in advanced clinical trials, we found that 17-AAG decreases invasion toward SVZ hNPC CM in vitro, but only at concentrations above 1 μM (Figure S6A). At high concentrations, 17-AAG also decreased DIPG cell viability (Figure S6B), as has been reported for other HSP90 inhibitors (Grasso et al., 2015). Brain penetration of 17-AAG has been measured at <1 μM in rodent models (Egorin et al., 2001), so we did not expect to find a therapeutic effect in vivo. Accordingly, we did not find a difference in SVZ invasion between mice that received 17-AAG following pontine xenograft compared to those receiving vehicle control (Figure S6C). Because HSP90 targeting with a more potent or brain penetrant antagonist may be a useful strategy, we sought proof of principle demonstration that HSP90 inhibition could decrease SVZ invasion. Stereotactic injection of shRNA-expressing lentivirus targeting the *Hsp90b1* gene into the mouse SVZ resulted in fewer DIPG cells invading the SVZ at 16 weeks following pontine xenograft, with no effect on initial tumor engraftment or SVZ NPC density (Figures S6D–S6H). These results support the concept that HSP90B is necessary for DIPG

(C) Size exclusion chromatography. UV trace (above) shows overall protein elution. All four proteins coeluted at approximately the 212 kDa size expected for a complex of all four proteins, illustrated by western blot (WB) analyses. Vertical lines demarcate separate WB gels placed side-by-side in image to show the sequence of elution fractions. For HSP90B, SPARC and PTN, three WB gels were run to accommodate all fractions. For SPARCL1, an additional WB gel was run at the same time and imaged in parallel to accommodate two elution fractions omitted at the time of loading. A row represents the WB for a given protein. A column represents a single elution fraction analyzed for each of the four proteins, immunostained separately. Size exclusion chromatography was performed once, and Westerns repeated in technical replicate.

(D) All four proteins copurified together in immunoprecipitation reactions for any one of the four proteins, more so than with a control IgG; performed with biological replicates. Three control proteins also present in SVZ hNPC CM—GRP78, IGFBP2, and BCAN—did not copurify with any of the four proteins.

(E) 9 out of a panel of 9 patient-derived glioma cultures (see Table S1) invade preferentially toward the combination of four proteins similarly to toward human SVZ NPC CM, compared to unconditioned hNPC medium. All experiments performed with n = 3 replicates/wells and analyzed by unpaired, two-tailed Student's t tests for comparison between unconditioned hNPC medium and either the combination of the four proteins or SVZ hNPC CM.

Data shown as mean ± SEM. *$p < 0.05$, **$p < 0.01$, ***$p < 0.001$.

See also Figure S3 and Table S1.

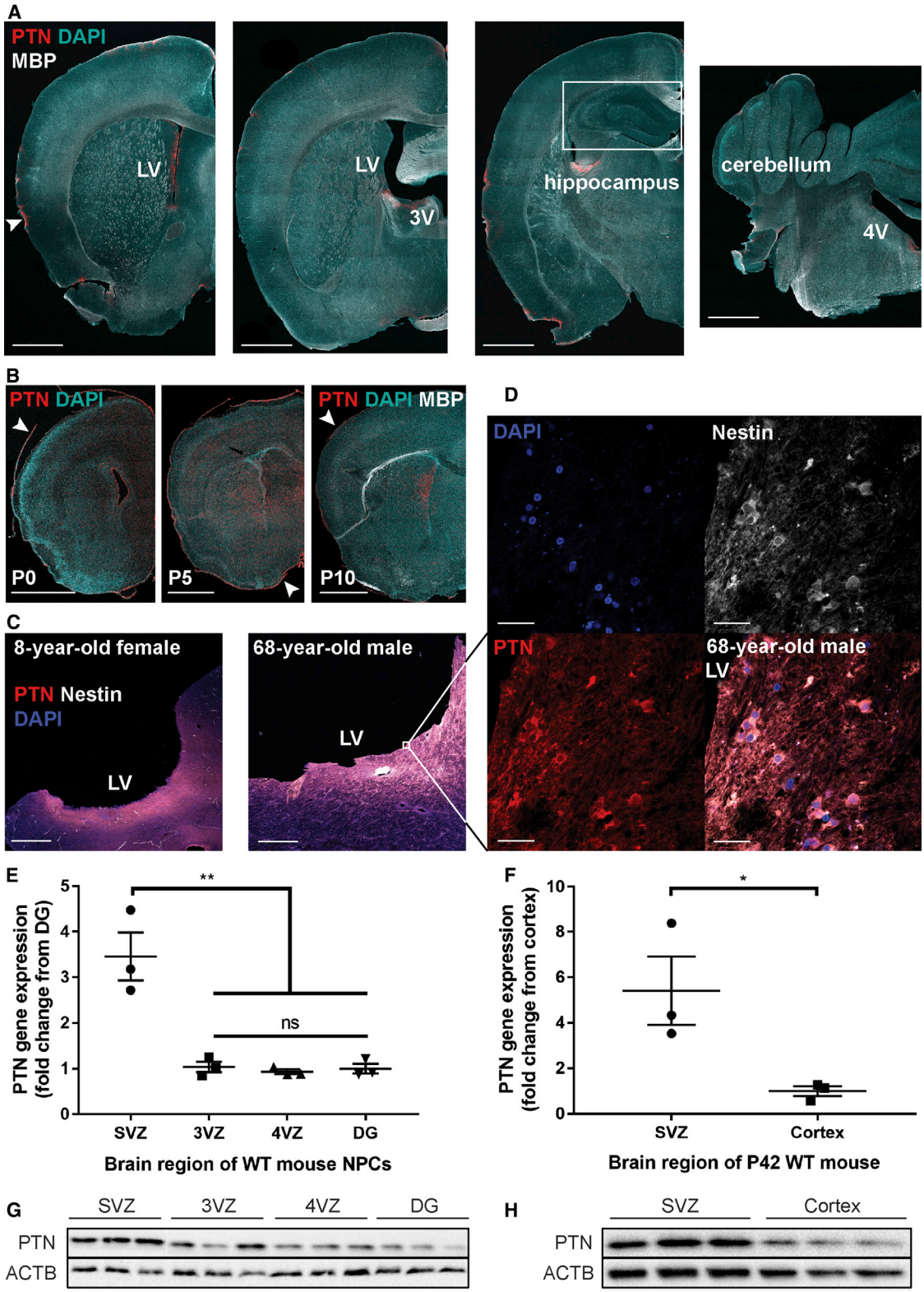

Figure 5. PTN Expression Is Enriched in the Postnatal SVZ

(A) PTN protein is highly localized to the SVZ and pia mater (white arrowhead) in the adult murine brain (left). PTN is expressed at lower levels in the 3VZ (left middle) and 4VZ (right), and is undetectable in the hippocampus (right middle). Scale bar, 1 mm. LV, lateral ventricle; 3V, third ventricle; 4V, fourth ventricle.

(legend continued on next page)

invasion of the SVZ and that effective HSP90 inhibition could prove a useful strategy.

NPC-Secreted Factors Activate the Rho/ROCK Pathway

The Rho/Rho kinase (ROCK) pathway is linked to PTN-PTPRZ signaling (Niisato et al., 2005; Tamura et al., 2006) and to tumor invasion in general (see Parri and Chiarugi, 2010 for review). To test the involvement of this pathway in DIPG invasion of the SVZ, we exposed DIPG cells to unconditioned hNPC medium or SVZ hNPC CM for a range of time points between 0.5–120 min and subsequently measured RhoA and ROCK activation. Exposure to SVZ hNPC CM for 1–5 min resulted in an increase in RhoA activation compared to exposure to unconditioned hNPC medium (Figure 7A). ROCK activation occurs at a later time point, after exposure to SVZ hNPC CM for 60–120 min (Figure 7B). Exposure to the PTN complex activated RhoA and ROCK at levels similar to exposure to SVZ hNPC CM (Figures 7C and 7D). DIPG cells with shRNA-mediated knock down of *PTPRZ1* exhibited abrogation of RhoA and ROCK activation when exposed to SVZ hNPC CM or the PTN complex, compared to scrambled control DIPG cells (Figure S7A), further supporting that PTN-PTPRZ signaling results in activation of the Rho/ROCK pathway. Exposure of DIPG cells to two different ROCK inhibitors decreased DIPG invasion toward SVZ hNPC CM (Figures 7E and 7F), without affecting cell viability (Figures S7B and S7C). These results implicate the involvement of the Rho/ROCK pathway in promoting DIPG invasion in response to the SVZ NPC-secreted PTN complex. Thus, DIPG cells originating in the pons invade widely throughout the brain, and when in proximity to SVZ NPCs, are drawn in to the SVZ by PTN and its three required binding partners (Figure 7G). NPC-secreted PTN and binding partners activate the Rho/ROCK pathway in DIPG cells, which promotes glioma cell migration and invasion (Figure 7H).

DISCUSSION

The present study demonstrates a pathogenic role for NPC:glioma interactions and defines glioma chemoattractants secreted by SVZ NPCs. While NPCs are known to migrate toward and track glioma cells (Aboody et al., 2000; Li et al., 2007) in response to glioma-secreted cytokines (Ehtesham et al., 2004; Imitola et al., 2004) and additional signals (An et al., 2009; Staflin et al., 2009), glioma migration/invasion toward NPC populations has been under recognized. Pleiotrophin, along with three required binding partners, mediates chemoattraction toward the SVZ. Pleiotrophin, specifically enriched in the SVZ after early postnatal neurodevelopment and secreted by SVZ NPCs, interacts with three additional proteins secreted by NPCs that together mediate invasion of a range of molecularly and clinically distinct glioma types and activates the Rho/ROCK pathway in glioma cells. Taken together, the findings presented here identify pleiotrophin and its binding partners as key chemoattractant proteins secreted by SVZ NPCs that are necessary and sufficient for glioma invasion of the SVZ niche.

Implications for Glioma

The SVZ is a site of frequent spread in HGG, and glioma spread to the SVZ is associated with decreased survival (Chaichana et al., 2008; Jafri et al., 2013; Mistry et al., 2017a, 2017b) and increased tumor recurrence (Adeberg et al., 2014; Chen et al., 2015). Notably, decreased survival and increased early recurrence in adult GBM are associated specifically with glioma contact of the lateral ventricle SVZ (Mistry et al., 2017b) for reasons that have yet to be fully elucidated. Ongoing clinical studies seek to improve outcomes by increasing the radiation dose to the SVZ in GBM patients, as retrospective analyses indicate that incidental radiation to the SVZ robustly correlates with progression-free survival (Chen et al., 2013; Evers et al., 2010; Lee et al., 2013). In DIPG, mortality typically results from brainstem disease, but spread to the SVZ can result in increased morbidity and mortality. As more effective disease control is achieved in the pons for children with DIPG, regions of distant spread such as the SVZ may emerge as a larger clinical problem.

Understanding DIPG invasion of the SVZ informs not only the pathobiology of this important pediatric cancer, but also clarifies mechanisms of SVZ involvement that are conserved across HGG types. DIPG travels some distance between its origins in the pons and the lateral ventricle SVZ. The pattern of DIPG spread found at the time of autopsy is widespread and multidirectional (Caretti et al., 2014), consistent with an intrinsic invasiveness of DIPG cells (Nagaraja et al., 2017) that may be exacerbated by factors in the local microenvironment such as 4VZ NPCs as above. When DIPG cells invade the forebrain, the demonstrated chemoattractant effect of SVZ NPCs may then act at short to medium range to draw invading cells to the SVZ niche. Additional growth-promoting factors present in the SVZ stem cell niche may function to encourage blooming of substantial masses when glioma cells arrive there.

Pleiotrophin Has Pleiotrophic Roles in Development and Cancer

Pleiotrophin (PTN), also known as heparin-binding growth-associated molecule, is a developmentally regulated, secreted growth factor with numerous and diverse roles in brain development,

(B) PTN protein expression near the lateral ventricles and in the pia (white arrowheads) in the postnatal murine brain at P0, P5, and P10. Scale bar, 1 mm.
(C) PTN protein is highly expressed in the human SVZ of an 8-year-old female (left) and a 68-year-old male (right). PTN protein co-localizes with Nestin$^+$ NPCs in the SVZ and is also present extracellularly. Scale bar, 1 mm.
(D) High-magnification images of PTN expression co-localizing with Nestin$^+$ NPCs in the SVZ of a 68-year-old male. Scale bar, 25 μm.
(E and G) *Ptn* gene (E) and PTN protein expression (G) are higher in SVZ mNPCs isolated from P14 wild-type (WT) mice, compared to 3VZ, 4VZ, or DG mNPCs isolated at the same age. Gene expression values shown are normalized to *Actb* expression. qPCR experiments performed with n = 3 wells of cells and analyzed by one-way ANOVA with Tukey post hoc adjustment for multiple comparisons.
(F and H) *Ptn* gene (F) and PTN protein expression (H) are higher in the SVZ compared to cortex of P42 mice. Gene expression values shown are normalized to *Actb* expression. qPCR experiments performed with n = 3 mice and analyzed by unpaired, two-tailed Student's t test.
Data shown as mean ± SEM. *$p < 0.05$, **$p < 0.01$.
See also Figure S4.

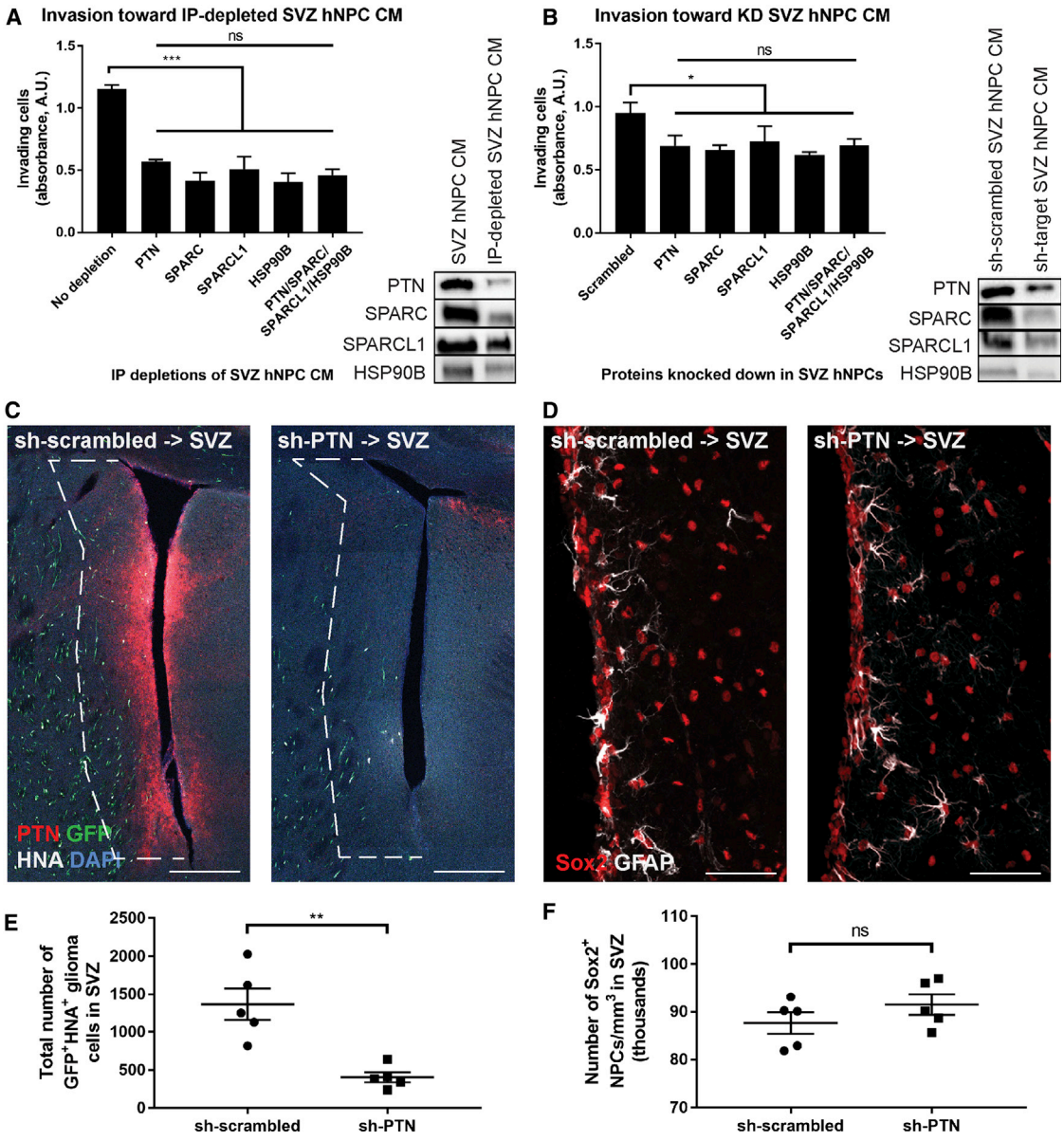

Figure 6. PTN Is Necessary for Glioma Invasion toward the SVZ

(A) DIPG cells invade less toward SVZ hNPC CM after immunodepletion of any or a combination of the four proteins. Depletion of target proteins was confirmed by western blot.

(B) DIPG cells invade less toward CM from SVZ hNPCs that had any or all of the four proteins knocked down by shRNA-expressing lentivirus, compared to CM from SVZ hNPCs expressing a scrambled shRNA control. Knock down efficacy was confirmed by western blot. In vitro experiments performed with n = 3 replicates/wells in SU-DIPG-XIII FL cells and analyzed by one-way ANOVA with Tukey post hoc adjustment for multiple comparisons.

(C and E) Fewer orthotopically xenografted GFP$^+$ HNA$^+$ SU-DIPG-XIII FL cells invaded the SVZ, defined as a 200 μm-wide region adjacent to the lateral ventricles (outlined in dashed white lines), when lentivirus expressing sh-*Ptn* (right) was injected into the SVZ, compared to lentivirus expressing a scrambled shRNA control (left). Scale bar, 200 μm (C). In vivo experiments performed with n = 5 mice per group. Stereological cell counts at 16 weeks following xenograft analyzed by unpaired, two-tailed Student's t test. Each data point = one mouse (E).

(D and F) The density of Sox2$^+$ NPCs in the SVZ was equivalent in mice injected with lentivirus expressing sh-*Ptn* (right) or scrambled shRNA control (left). Scale bar, 50 μm (D). In vivo experiments performed with n = 5 mice per group. Stereological cell counts at 16 weeks following xenograft analyzed by unpaired, two-tailed Student's t test. Each data point = one mouse (F).

Data shown as mean ± SEM. *p < 0.05, **p < 0.01, ***p < 0.001.

See also Figures S5 and S6.

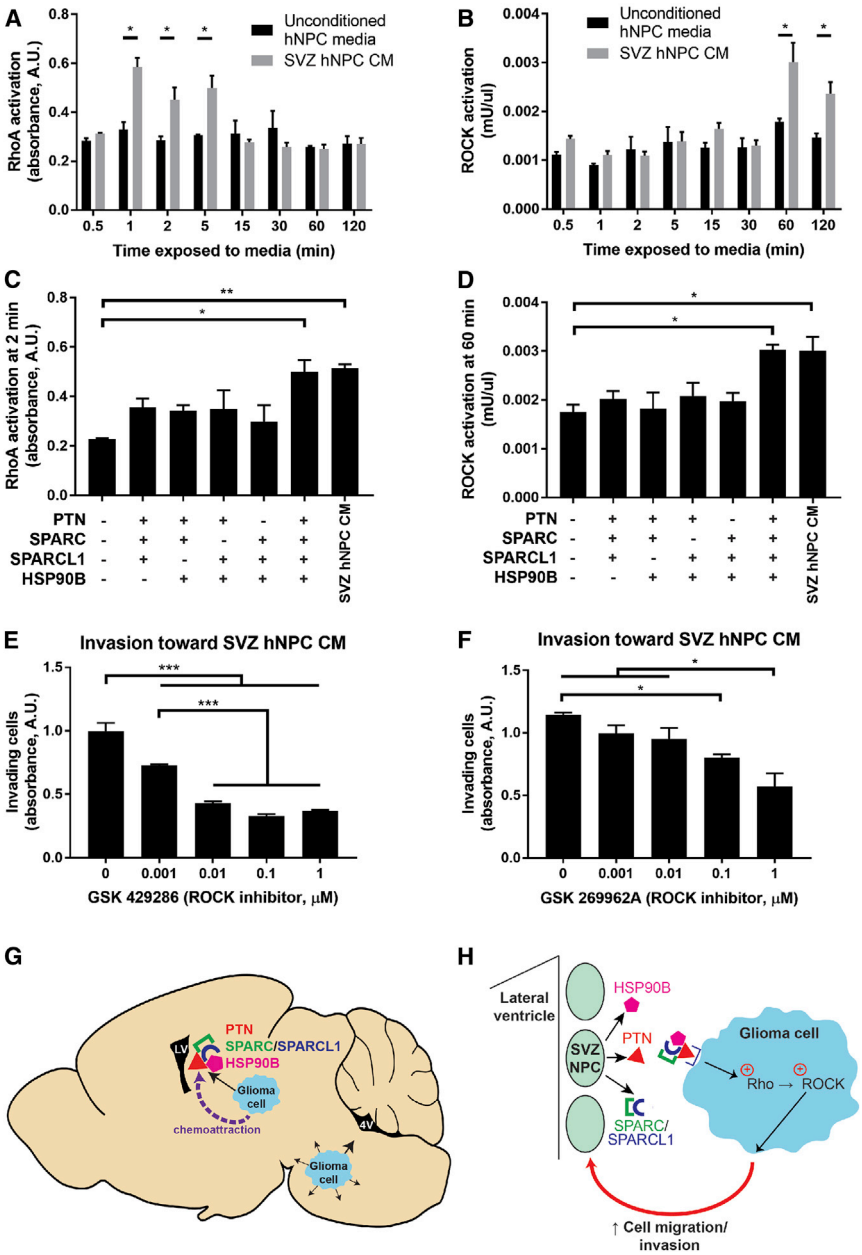

Figure 7. NPC-Secreted Factors Activate the Rho/ROCK Pathway

(A and B) Exposure of DIPG cells to SVZ hNPC CM activated RhoA after 1–5 min (A) and ROCK after 60–120 min (B), compared to unconditioned hNPC medium.

(C and D) Exposure to PTN and the three binding partners in unconditioned hNPC medium activated RhoA (C) and ROCK (D) similarly to SVZ hNPC CM.

(E and F) Treatment with ROCK inhibitors GSK 429286 (E) or GSK 269962A (F) decreased DIPG invasion toward SVZ hNPC CM in a dose-dependent manner.

(G) Schematic illustrating the model of glioma cells originating in the pons invading generally in the ventral pons, and being drawn at short to medium range into the SVZ upon exposure to PTN and the three binding partners secreted by SVZ NPCs.

(H) Schematic illustrating the model of glioma chemoattraction toward NPC-secreted PTN and the three binding partners, subsequent activation of the Rho/ROCK pathway in glioma cells, and promotion of glioma cell migration and invasion.

All experiments performed with n = 3 replicates/wells in SU-DIPG-XIII FL cells and analyzed by unpaired two-tailed Student's t tests for comparison between unconditioned and conditioned hNPC medium (A and B) or by one-way ANOVA with Tukey post hoc adjustment for multiple comparisons (C–F). Data shown as mean ± SEM. *$p < 0.05$, **$p < 0.01$, ***$p < 0.001$.

See also Figure S7.

homeostasis, and regeneration. Pleiotrophin has several possible receptors, including protein tyrosine phosphatase receptor type ζ (PTPRZ), anaplastic lymphoma kinase (ALK), N-syndecan, neuroglycan, integrin αvβ3, and lipoprotein receptor-related protein (LRP) (González-Castillo et al., 2015), and as such, the functional effects of pleiotrophin binding are cell context-specific. Pleiotrophin was originally recognized to promote neurite outgrowth (Kinnunen et al., 1999; Li et al., 1990; Rauvala and Pihlaskari, 1987) and subsequently found to promote haptotactic neuroblast migration along radial glial processes from the subventricular germinal zone to the developing cortical plate during corticogenesis (Maeda and Noda, 1998). Additional functions of pleiotrophin range from supporting dendrite and axonal regeneration (Blondet et al., 2005; Mi et al., 2007) to modulation of synaptic plasticity (Lauri et al., 1998; Pavlov et al., 2002). Pleiotrophin and PTPRZ are both highly expressed in human white matter oligodendroglial precursor cells (OPCs), and PTN-PTPRZ signaling promotes postnatal OPC differentiation during developmental myelination and remyelination after injury (Harroch et al., 2002; Sim et al., 2006). In prenatal human OPCs, PTN-PTPRZ signaling promotes proliferation, population expansion, and self-renewal through downstream regulation of the Wnt pathway (McClain et al., 2012). Underscoring the broad roles for pleiotrophin in neurodevelopment, pleiotrophin knockout mice exhibit aberrant cognitive behavior as well as anomalies in corticogenesis (Hienola et al., 2004; Krellman et al., 2014).

Here, we show that after development, pleiotrophin expression is highly enriched in the murine and human SVZ. The identification of pleiotrophin as a protein secreted by murine and human SVZ NPCs is consistent with reports identifying PTN in the secretomes of various neural stem cell populations (Furuta et al., 2004; Lee et al., 2012). While this suggests a role for pleiotrophin in the postnatal SVZ niche, the in vivo function of pleiotrophin and the reasons for its elevated expression in the

SVZ compared to other neural stem cell niches remain to be fully elucidated.

In addition to its roles in normal neurodevelopment, plasticity, and regeneration, pleiotrophin also has many roles in cancer, including involvement in tumor growth (Tsirmoula et al., 2012; Wellstein et al., 1992) and invasion and metastasis (Czubayko et al., 1996; Wu et al., 2005). Pleiotrophin is expressed by HGG cells, and expression levels are inversely correlated with overall patient survival (Zhang et al., 2015). Autocrine/paracrine secretion of pleiotrophin promotes adult GBM migration via PTN-PTPRZ signaling (Lu et al., 2005; Ulbricht et al., 2003). Like neuroblasts during corticogenesis (Maeda and Noda, 1998), GBM cells exhibit robust haptotactic migration toward immobilized pleiotrophin, but only show weak chemotactic migration toward free soluble pleiotrophin (Lu et al., 2005; Ulbricht et al., 2003). The finding here that NPC-secreted pleiotrophin requires three binding partners may reflect a similar requirement for immobilization to encourage haptotactic migration into the SVZ.

The Rho/ROCK Pathway in Glioma Migration and Invasion

Rho/Rho kinase (ROCK) signaling is a well-established pathway in cell migration. It is a complex pathway, and its role in glioma migration and invasion may be context-specific. In normal cell migration, active ROCK promotes the LIM kinase/cofilin pathway, thereby promoting stabilization of actin filaments (Maekawa et al., 1999; Sumi et al., 2001). In a parallel pathway, active ROCK inhibits myosin light chain phosphatase, thus promoting actin and myosin crosslinking. This leads to contraction of the trailing edge and forward motion of the cell and thereby increases cell migration (Mitchison and Cramer, 1996). Consistent with the potential pro-motility effects of modulating Rho/ROCK pathway activity in either direction, the role of Rho/ROCK in glioma migration and invasion is complex and seemingly contradictory. Some studies found that inhibition of ROCK decreased glioma migration (Lin et al., 2009; Oellers et al., 2009), while another study found that inhibition of ROCK increased glioma migration and invasion (Salhia et al., 2005). Here, we find that pleiotrophin and its binding partners activate the Rho/ROCK pathway in glioma cells, and treatment with ROCK inhibitors decreases their invasion toward factors secreted by SVZ NPCs, thus implicating this prominent migration pathway in glioma invasion of the SVZ.

Neurite Outgrowth and Axon Guidance Molecules in Glioma Invasion

An emerging theme in glioma pathobiology is malignant hijacking of neurodevelopmental mechanisms (see Baker et al., 2015 for review), including the re-purposing of traditional neurite outgrowth and axon guidance molecules to regulate glioma invasion. One major family of axon guidance molecules, the ephrins and Eph receptors, promote migration and invasion in adult GBM (Nakada et al., 2010; Sikkema et al., 2012) and in DIPG (Nagaraja et al., 2017). Netrins are another class of chemoattractant cues for pathfinding axons that promote GBM invasion (Shimizu et al., 2013). On the other hand, signals that are chemorepulsive to the axonal growth cone prove inhibitory to glioma invasion. SLIT/ROBO signaling, canonically involved in axon pathfinding as a chemorepulsive ligand-receptor system (Brose et al., 1999; Kidd et al., 1999), functions similarly as a chemorepellant in glioma (Mertsch et al., 2008). Semaphorins function chiefly as short-range inhibitory signals for developing axons, and HGGs express both semaphorins and the receptors plexins and neuropilins (Rieger et al., 2003); semaphorin signaling has been found to limit glioma motility (Li and Lee, 2010; Zhou et al., 2012).

As a molecule that promotes neurite outgrowth and neuroblast migration, pleiotrophin appears to similarly promote glioma tropism toward a preferred niche. Identification of pleiotrophin and its binding partners as chemoattractant factors secreted by NPCs begins to explain how and why glioma cells preferentially invade the SVZ. Targeting the pleiotrophin complex, including HSP90 inhibition, and downstream Rho/ROCK signaling emerge as therapeutic strategies to limit or prevent tumor invasion of the SVZ in high-grade gliomas.

STAR★METHODS

Detailed methods are provided in the online version of this paper and include the following:

- KEY RESOURCES TABLE
- CONTACT FOR REAGENT AND RESOURCE SHARING
- EXPERIMENTAL MODEL AND SUBJECT DETAILS
  - Mice and housing conditions
  - Patient-derived glioma cell culture
  - Neural precursor cell culture and generation of conditioned medium
  - Neuron culture and generation of conditioned medium
  - Culture of CHL-1 melanoma cells
  - Orthotopic xenografting and lentiviral injections
  - Human SVZ samples
- METHOD DETAILS
  - Bioluminescent IVIS imaging
  - Drug treatment of mice
  - Perfusion and immunohistochemistry
  - Analysis of tumor spread over time
  - Matrigel invasion assay
  - Biochemical assays
  - Two-dimensional gel electrophoresis
  - Protein identification by mass spectrometry
  - Recombinant proteins used
  - Size exclusion chromatography
  - Immunoprecipitation
  - Western blot analysis
  - Dissection of mouse SVZ and cortex
  - qPCR
  - shRNA-expressing lentivirus preparation and infection
  - RhoA and ROCK activation assays
  - Pharmacologic inhibition
  - Whole exome sequencing
  - RNA sequencing
  - CellTiter-Glo assay
- QUANTIFICATION AND STATISTICAL ANALYSIS
  - Stereological cell counting
  - Statistical analyses

- DATA AND SOFTWARE AVAILABILITY
  - Patient-derived cell cultures
  - Sequencing data
  - Raw data and statistics

SUPPLEMENTAL INFORMATION

Supplemental Information includes seven figures and one table and can be found with this article online at http://dx.doi.org/10.1016/j.cell.2017.07.016.

An audio PaperClip is available at http://dx.doi.org/10.1016/j.cell.2017.07.016#mmc2.

AUTHOR CONTRIBUTIONS

Conceptualization, E.Y.Q. and M.M.; Methodology, E.Y.Q., P.K.J., and M.M.; Investigation, E.Y.Q., D.D.C., K.L.A., J.L., S.N., A.M., and H.V.; Writing – Original Draft, E.Y.Q. and M.M.; Writing – Review & Editing, E.Y.Q., J.L., S.N., P.K.J., and M.M.; Funding Acquisition, C.J. and M.M.; Supervision, P.K.J., C.J., and M.M.

ACKNOWLEDGMENTS

The authors gratefully acknowledge support from the Childhood Brain Tumor Foundation, Lyla Nsouli Foundation, Unravel Pediatric Cancer, National Institute of Neurological Disorders and Stroke (R01NS092597), Liwei Wang Research Fund, Reller Family Research Fund, Department of Defense (W81XWH-151-0131), McKenna Claire Foundation, Alex's Lemonade Stand Foundation, The Cure Starts Now Foundation and DIPG Collaborative, N8 Foundation, California Institute for Regenerative Medicine (RN3-06510), V Foundation, Joey Fabus Childhood Cancer Foundation, Wayland Villars DIPG Foundation, Connor Johnson, Zoey Ganesh, and Declan Gloster Memorial Funds, Virginia and D.K. Ludwig Fund for Cancer Research, Child Health Research Institute at Stanford, Anne T. and Robert M. Bass Endowed Faculty Scholarship in Pediatric Cancer and Blood Diseases, and Cancer Research UK (C13468/A13982 and C13468/A23536).

Received: March 5, 2017
Revised: June 15, 2017
Accepted: July 13, 2017
Published: August 17, 2017

REFERENCES

Aboody, K.S., Brown, A., Rainov, N.G., Bower, K.A., Liu, S., Yang, W., Small, J.E., Herrlinger, U., Ourednik, V., Black, P.M., et al. (2000). Neural stem cells display extensive tropism for pathology in adult brain: evidence from intracranial gliomas. Proc. Natl. Acad. Sci. USA *97*, 12846–12851.

Adeberg, S., König, L., Bostel, T., Harrabi, S., Welzel, T., Debus, J., and Combs, S.E. (2014). Glioblastoma recurrence patterns after radiation therapy with regard to the subventricular zone. Int. J. Radiat. Oncol. Biol. Phys. *90*, 886–893.

An, J.H., Lee, S.Y., Jeon, J.Y., Cho, K.G., Kim, S.U., and Lee, M.A. (2009). Identification of gliotropic factors that induce human stem cell migration to malignant tumor. J. Proteome Res. *8*, 2873–2881.

Ashburner, M., Ball, C.A., Blake, J.A., Botstein, D., Butler, H., Cherry, J.M., Davis, A.P., Dolinski, K., Dwight, S.S., Eppig, J.T., et al.; The Gene Ontology Consortium (2000). Gene ontology: tool for the unification of biology. Nat. Genet. *25*, 25–29.

Baker, S.J., Ellison, D.W., and Gutmann, D.H. (2015). Pediatric gliomas as neurodevelopmental disorders. Glia *64*, 879–895.

Beaudoin, G.M.J., 3rd, Lee, S.-H., Singh, D., Yuan, Y., Ng, Y.-G., Reichardt, L.F., and Arikkath, J. (2012). Culturing pyramidal neurons from the early postnatal mouse hippocampus and cortex. Nat. Protoc. *7*, 1741–1754.

Blondet, B., Carpentier, G., Lafdil, F., and Courty, J. (2005). Pleiotrophin cellular localization in nerve regeneration after peripheral nerve injury. J. Histochem. Cytochem. *53*, 971–977.

Brose, K., Bland, K.S., Wang, K.H., Arnott, D., Henzel, W., Goodman, C.S., Tessier-Lavigne, M., and Kidd, T. (1999). Slit proteins bind Robo receptors and have an evolutionarily conserved role in repulsive axon guidance. Cell *96*, 795–806.

Caretti, V., Bugiani, M., Freret, M., Schellen, P., Jansen, M., van Vuurden, D., Kaspers, G., Fisher, P.G., Hulleman, E., Wesseling, P., et al. (2014). Subventricular spread of diffuse intrinsic pontine glioma. Acta Neuropathol. *128*, 605–607.

Chaichana, K.L., McGirt, M.J., Frazier, J., Attenello, F., Guerrero-Cazares, H., and Quinones-Hinojosa, A. (2008). Relationship of glioblastoma multiforme to the lateral ventricles predicts survival following tumor resection. J. Neurooncol. *89*, 219–224.

Chen, L., Guerrero-Cazares, H., Ye, X., Ford, E., McNutt, T., Kleinberg, L., Lim, M., Chaichana, K., Quinones-Hinojosa, A., and Redmond, K. (2013). Increased subventricular zone radiation dose correlates with survival in glioblastoma patients after gross total resection. Int. J. Radiat. Oncol. Biol. Phys. *86*, 616–622.

Chen, L., Chaichana, K.L., Kleinberg, L., Ye, X., Quinones-Hinojosa, A., and Redmond, K. (2015). Glioblastoma recurrence patterns near neural stem cell regions. Radiother. Oncol. *116*, 294–300.

Czubayko, F., Schulte, A.M., Berchem, G.J., and Wellstein, A. (1996). Melanoma angiogenesis and metastasis modulated by ribozyme targeting of the secreted growth factor pleiotrophin. Proc. Natl. Acad. Sci. USA *93*, 14753–14758.

Donaldson, S.S., Laningham, F., and Fisher, P.G. (2006). Advances toward an understanding of brainstem gliomas. J Clin Oncol. *24*, 1266–1272.

Egorin, M.J., Zuhowski, E.G., Rosen, D.M., Sentz, D.L., Covey, J.M., and Eiseman, J.L. (2001). Plasma pharmacokinetics and tissue distribution of 17-(allylamino)-17-demethoxygeldanamycin (NSC 330507) in CD2F1 mice1. Cancer Chemother. Pharmacol. *47*, 291–302.

Ehtesham, M., Yuan, X., Kabos, P., Chung, N.H., Liu, G., Akasaki, Y., Black, K.L., and Yu, J.S. (2004). Glioma tropic neural stem cells consist of astrocytic precursors and their migratory capacity is mediated by CXCR4. Neoplasia *6*, 287–293.

Evers, P., Lee, P.P., DeMarco, J., Agazaryan, N., Sayre, J.W., Selch, M., and Pajonk, F. (2010). Irradiation of the potential cancer stem cell niches in the adult brain improves progression-free survival of patients with malignant glioma. BMC Cancer *10*, 384.

Furuta, M., Shiraishi, T., Okamoto, H., Mineta, T., Tabuchi, K., and Shiwa, M. (2004). Identification of pleiotrophin in conditioned medium secreted from neural stem cells by SELDI-TOF and SELDI-tandem mass spectrometry. Brain Res. Dev. Brain Res. *152*, 189–197.

González-Castillo, C., Ortuño-Sahagún, D., Guzmán-Brambila, C., Pallàs, M., and Rojas-Mayorquín, A.E. (2015). Pleiotrophin as a central nervous system neuromodulator, evidences from the hippocampus. Front. Cell. Neurosci. *8*, 443.

Grasso, C.S., Tang, Y., Truffaux, N., Berlow, N.E., Liu, L., Debily, M.-A., Quist, M.J., Davis, L.E., Huang, E.C., Woo, P.J., et al. (2015). Functionally defined therapeutic targets in diffuse intrinsic pontine glioma. Nat. Med. *21*, 555–559.

Harroch, S., Furtado, G.C., Brueck, W., Rosenbluth, J., Lafaille, J., Chao, M., Buxbaum, J.D., and Schlessinger, J. (2002). A critical role for the protein tyrosine phosphatase receptor type Z in functional recovery from demyelinating lesions. Nat. Genet. *32*, 411–414.

Hienola, A., Pekkanen, M., Raulo, E., Vanttola, P., and Rauvala, H. (2004). HB-GAM inhibits proliferation and enhances differentiation of neural stem cells. Mol. Cell. Neurosci. *26*, 75–88.

Imitola, J., Raddassi, K., Park, K.I., Mueller, F.-J.F.-J., Nieto, M., Teng, Y.D., Frenkel, D., Li, J., Sidman, R.L., Walsh, C.A., et al. (2004). Directed migration of neural stem cells to sites of CNS injury by the stromal cell-derived factor 1alpha/CXC chemokine receptor 4 pathway. Proc. Natl. Acad. Sci. USA *101*, 18117–18122.

Jafri, N.F., Clarke, J.L., Weinberg, V., Barani, I.J., and Cha, S. (2013). Relationship of glioblastoma multiforme to the subventricular zone is associated with survival. Neuro-oncol. *15*, 91–96.

Kidd, T., Bland, K.S., and Goodman, C.S. (1999). Slit is the midline repellent for the robo receptor in Drosophila. Cell *96*, 785–794.

Kim, D., Pertea, G., Trapnell, C., Pimentel, H., Kelley, R., and Salzberg, S.L. (2013). TopHat2: accurate alignment of transcriptomes in the presence of insertions, deletions and gene fusions. Genome Biol. *14*, R36.

Kinnunen, A., Niemi, M., Kinnunen, T., Kaksonen, M., Nolo, R., and Rauvala, H. (1999). Heparan sulphate and HB-GAM (heparin-binding growth-associated molecule) in the development of the thalamocortical pathway of rat brain. Eur. J. Neurosci. *11*, 491–502.

Krellman, J.W., Ruiz, H.H., Marciano, V.A., Mondrow, B., and Croll, S.D. (2014). Behavioral and neuroanatomical abnormalities in pleiotrophin knockout mice. PLoS ONE *9*, e100597.

Lane, T.F., and Sage, E.H. (1994). The biology of SPARC, a protein that modulates cell-matrix interactions. FASEB J. *8*, 163–173.

Lauri, S.E., Rauvala, H., Kaila, K., and Taira, T. (1998). Effect of heparin-binding growth-associated molecule (HB-GAM) on synaptic transmission and early LTP in rat hippocampal slices. Eur. J. Neurosci. *10*, 188–194.

Lee, C., Hu, J., Ralls, S., Kitamura, T., Loh, Y.P., Yang, Y., Mukouyama, Y.S., Ahn, S., et al. (2012). The molecular profiles of neural stem cell niche in the adult subventricular zone. PLoS ONE *7*, e50501.

Lee, P., Eppinga, W., Lagerwaard, F., Cloughesy, T., Slotman, B., Nghiemphu, P.L., Wang, P.-C., Kupelian, P., Agazaryan, N., Demarco, J., et al. (2013). Evaluation of high ipsilateral subventricular zone radiation therapy dose in glioblastoma: a pooled analysis. Int. J. Radiat. Oncol. Biol. Phys. *86*, 609–615.

Li, X., and Lee, A.Y.W. (2010). Semaphorin 5A and plexin-B3 inhibit human glioma cell motility through RhoGDIalpha-mediated inactivation of Rac1 GTPase. J. Biol. Chem. *285*, 32436–32445.

Li, Y.S., Milner, P.G., Chauhan, A.K., Watson, M.A., Hoffman, R.M., Kodner, C.M., Milbrandt, J., and Deuel, T.F. (1990). Cloning and expression of a developmentally regulated protein that induces mitogenic and neurite outgrowth activity. Science *250*, 1690–1694.

Li, S., Gao, Y., Tokuyama, T., Yamamoto, J., Yokota, N., Yamamoto, S., Terakawa, S., Kitagawa, M., and Namba, H. (2007). Genetically engineered neural stem cells migrate and suppress glioma cell growth at distant intracranial sites. Cancer Lett. *251*, 220–227.

Liao, Y., Smyth, G.K., and Shi, W. (2014). featureCounts: an efficient general purpose program for assigning sequence reads to genomic features. Bioinformatics *30*, 923–930.

Lin, G.L., and Monje, M. (2017). A protocol for rapid post-mortem cell culture of diffuse intrinsic pontine glioma (DIPG). J. Vis. Exp. http://dx.doi.org/10.3791/55360.

Lin, C.-C., Chen, J.-T., Yang, J.-S., Lu, H.-F., Hsu, S.-C., Tan, T.-W., Lin, Y.-T., Ma, Y.-S., Ip, S.-W., Wu, J.-J., et al. (2009). Danthron inhibits the migration and invasion of human brain glioblastoma multiforme cells through the inhibition of mRNA expression of focal adhesion kinase, Rho kinases-1 and metalloproteinase-9. Oncol. Rep. *22*, 1033–1037.

Louis, D.N., Perry, A., Reifenberger, G., von Deimling, A., Figarella-Branger, D., Cavenee, W.K., Ohgaki, H., Wiestler, O.D., Kleihues, P., and Ellison, D.W. (2016). The 2016 World Health Organization Classification of Tumors of the Central Nervous System: a summary. Acta Neuropathol. *131*, 803–820.

Love, M.I., Huber, W., and Anders, S. (2014). Moderated estimation of fold change and dispersion for RNA-seq data with DESeq2. Genome Biol. *15*, 550.

Lu, K.V., Jong, K.A., Kim, G.Y., Singh, J., Dia, E.Q., Yoshimoto, K., Wang, M.Y., Cloughesy, T.F., Nelson, S.F., and Mischel, P.S. (2005). Differential induction of glioblastoma migration and growth by two forms of pleiotrophin. J. Biol. Chem. *280*, 26953–26964.

Maeda, N., and Noda, M. (1998). Involvement of receptor-like protein tyrosine phosphatase zeta/RPTPbeta and its ligand pleiotrophin/heparin-binding growth-associated molecule (HB-GAM) in neuronal migration. J Cell Biol. *142*, 203–216.

Maekawa, M., Ishizaki, T., Boku, S., Watanabe, N., Fujita, A., Iwamatsu, A., Obinata, T., Ohashi, K., Mizuno, K., and Narumiya, S. (1999). Signaling from Rho to the actin cytoskeleton through protein kinases ROCK and LIM-kinase. Science *285*, 895–898.

McClain, C.R., Sim, F.J., and Goldman, S.A. (2012). Pleiotrophin suppression of receptor protein tyrosine phosphatase-β/ζ maintains the self-renewal competence of fetal human oligodendrocyte progenitor cells. J. Neurosci. *32*, 15066–15075.

Mertsch, S., Schmitz, N., Jeibmann, A., Geng, J.-G., Paulus, W., and Senner, V. (2008). Slit2 involvement in glioma cell migration is mediated by Robo1 receptor. J. Neurooncol. *87*, 1–7.

Mi, R., Chen, W., and Höke, A. (2007). Pleiotrophin is a neurotrophic factor for spinal motor neurons. Proc. Natl. Acad. Sci. USA *104*, 4664–4669.

Mistry, A.M., Hale, A.T., Chambless, L.B., Weaver, K.D., Thompson, R.C., and Ihrie, R.A. (2017a). Influence of glioblastoma contact with the lateral ventricle on survival: a meta-analysis. J. Neurooncol. *131*, 125–133.

Mistry, A.M., Dewan, M.C., White-Dzuro, G.A., Brinson, P.R., Weaver, K.D., Thompson, R.C., Ihrie, R.A., and Chambless, L.B. (2017b). Decreased survival in glioblastomas is specific to contact with the ventricular-subventricular zone, not subgranular zone or corpus callosum. J. Neurooncol. *132*, 341–349.

Mitchison, T.J., and Cramer, L.P. (1996). Actin-based cell motility and cell locomotion. Cell *84*, 371–379.

Monje, M., Mitra, S.S., Freret, M.E., Raveh, T.B., Kim, J., Masek, M., Attema, J.L., Li, G., Haddix, T., Edwards, M.S.B., et al. (2011). Hedgehog-responsive candidate cell of origin for diffuse intrinsic pontine glioma. Proc. Natl. Acad. Sci. USA *108*, 4453–4458.

Müller, S., Kunkel, P., Lamszus, K., Ulbricht, U., Lorente, G.A., Nelson, A.M., von Schack, D., Chin, D.J., Lohr, S.C., Westphal, M., and Melcher, T. (2003). A role for receptor tyrosine phosphatase ζ in glioma cell migration. Oncogene *22*, 6661–6668.

Nagaraja, S., Vitanza, N.A., Woo, P.J., Taylor, K.R., Liu, F., Zhang, L., Li, M., Meng, W., Ponnuswami, A., Sun, W., et al. (2017). Transcriptional dependencies in diffuse intrinsic pontine glioma. Cancer Cell *31*, 635–652.

Nakada, M., Anderson, E.M., Demuth, T., Nakada, S., Reavie, L.B., Drake, K.L., Hoelzinger, D.B., and Berens, M.E. (2010). The phosphorylation of ephrin-B2 ligand promotes glioma cell migration and invasion. Int. J. Cancer *126*, 1155–1165.

Niisato, K., Fujikawa, A., Komai, S., Shintani, T., Watanabe, E., Sakaguchi, G., Katsuura, G., Manabe, T., and Noda, M. (2005). Age-dependent enhancement of hippocampal long-term potentiation and impairment of spatial learning through the Rho-associated kinase pathway in protein tyrosine phosphatase receptor type Z-deficient mice. J. Neurosci. *25*, 1081–1088.

Oellers, P., Schröer, U., Senner, V., Paulus, W., and Thanos, S. (2009). ROCKs are expressed in brain tumors and are required for glioma-cell migration on myelinated axons. Glia *57*, 499–509.

Parri, M., and Chiarugi, P. (2010). Rac and Rho GTPases in cancer cell motility control. Cell Commun. Signal. *8*, 23.

Pavlov, I., Võikar, V., Kaksonen, M., Lauri, S.E., Hienola, A., Taira, T., and Rauvala, H. (2002). Role of heparin-binding growth-associated molecule (HB-GAM) in hippocampal LTP and spatial learning revealed by studies on overexpressing and knockout mice. Mol. Cell. Neurosci. *20*, 330–342.

Rauvala, H., and Pihlaskari, R. (1987). Isolation and some characteristics of an adhesive factor of brain that enhances neurite outgrowth in central neurons. J. Biol. Chem. *262*, 16625–16635.

Rieger, J., Wick, W., and Weller, M. (2003). Human malignant glioma cells express semaphorins and their receptors, neuropilins and plexins. Glia *42*, 379–389.

Salhia, B., Rutten, F., Nakada, M., Beaudry, C., Berens, M., Kwan, A., and Rutka, J.T. (2005). Inhibition of Rho-kinase affects astrocytoma morphology, motility, and invasion through activation of Rac1. Cancer Res. *65*, 8792–8800.

Sanai, N., Tramontin, A.D., Quiñones-Hinojosa, A., Barbaro, N.M., Gupta, N., Kunwar, S., Lawton, M.T., McDermott, M.W., Parsa, A.T., Manuel-García

Verdugo, J., et al. (2004). Unique astrocyte ribbon in adult human brain contains neural stem cells but lacks chain migration. Nature *427*, 740–744.

Shimizu, A., Nakayama, H., Wang, P., König, C., Akino, T., Sandlund, J., Coma, S., Italiano, J.E., Jr., Mammoto, A., Bielenberg, D.R., and Klagsbrun, M. (2013). Netrin-1 promotes glioblastoma cell invasiveness and angiogenesis by multiple pathways including activation of RhoA, cathepsin B, and cAMP-response element-binding protein. J. Biol. Chem. *288*, 2210–2222.

Sikkema, A.H., den Dunnen, W.F.A., Hulleman, E., van Vuurden, D.G., Garcia-Manero, G., Yang, H., Scherpen, F.J.G., Kampen, K.R., Hoving, E.W., Kamps, W.A., et al. (2012). EphB2 activity plays a pivotal role in pediatric medulloblastoma cell adhesion and invasion. Neuro-oncol. *14*, 1125–1135.

Sim, F.J., Lang, J.K., Waldau, B., Roy, N.S., Schwartz, T.E., Pilcher, W.H., Chandross, K.J., Natesan, S., Merrill, J.E., and Goldman, S.A. (2006). Complementary patterns of gene expression by human oligodendrocyte progenitors and their environment predict determinants of progenitor maintenance and differentiation. Ann. Neurol. *59*, 763–779.

Staflin, K., Zuchner, T., Honeth, G., Darabi, A., and Lundberg, C. (2009). Identification of proteins involved in neural progenitor cell targeting of gliomas. BMC Cancer *9*, 206.

Sumi, T., Matsumoto, K., Shibuya, A., and Nakamura, T. (2001). Activation of LIM kinases by myotonic dystrophy kinase-related Cdc42-binding kinase alpha. J. Biol. Chem. *276*, 23092–23096.

Tamura, H., Fukada, M., Fujikawa, A., and Noda, M. (2006). Protein tyrosine phosphatase receptor type Z is involved in hippocampus-dependent memory formation through dephosphorylation at Y1105 on p190 RhoGAP. Neurosci. Lett. *399*, 33–38.

Tsirmoula, S., Dimas, K., Hatziapostolou, M., Lamprou, M., Ravazoula, P., and Papadimitriou, E. (2012). Implications of pleiotrophin in human PC3 prostate cancer cell growth in vivo. Cancer Sci. *103*, 1826–1832.

Ulbricht, U., Brockmann, M.A., Aigner, A., Eckerich, C., Müller, S., Fillbrandt, R., Westphal, M., and Lamszus, K. (2003). Expression and function of the receptor protein tyrosine phosphatase zeta and its ligand pleiotrophin in human astrocytomas. J. Neuropathol. Exp. Neurol. *62*, 1265–1275.

Venkatesh, H.S., Johung, T.B., Caretti, V., Noll, A., Tang, Y., Nagaraja, S., Gibson, E.M., Mount, C.W., Polepalli, J., Mitra, S.S., et al. (2015). Neuronal activity promotes glioma growth through neuroligin-3 secretion. Cell *161*, 803–816.

Walker, T.L., and Kempermann, G. (2014). One mouse, two cultures: isolation and culture of adult neural stem cells from the two neurogenic zones of individual mice. J. Vis. Exp. http://dx.doi.org/10.3791/51225.

Wellstein, A., Fang, W.J., Khatri, A., Lu, Y., Swain, S.S., Dickson, R.B., Sasse, J., Riegel, A.T., and Lippman, M.E. (1992). A heparin-binding growth factor secreted from breast cancer cells homologous to a developmentally regulated cytokine. J. Biol. Chem. *267*, 2582–2587.

Wiech, H., Buchner, J., Zimmermann, R., and Jakob, U. (1992). Hsp90 chaperones protein folding in vitro. Nature *358*, 169–170.

Wu, H., Barusevicius, A., Babb, J., Klein-Szanto, A., Godwin, A., Elenitsas, R., Gelfand, J.M., Lessin, S., and Seykora, J.T. (2005). Pleiotrophin expression correlates with melanocytic tumor progression and metastatic potential. J. Cutan. Pathol. *32*, 125–130.

Zhang, L., Kundu, S., Feenstra, T., Li, X., Jin, C., Laaniste, L., El Hassan, T.E.A., Ohlin, K.E., Yu, D., Olofsson, T., et al. (2015). Pleiotrophin promotes vascular abnormalization in gliomas and correlates with poor survival in patients with astrocytomas. Sci. Signal. *8*, ra125.

Zhou, X., Ma, L., Li, J., Gu, J., Shi, Q., and Yu, R. (2012). Effects of SEMA3G on migration and invasion of glioma cells. Oncol. Rep. *28*, 269–275.

STAR★METHODS

KEY RESOURCES TABLE

REAGENT or RESOURCE	SOURCE	IDENTIFIER
Antibodies		
Mouse anti-human nuclei clone 235-1	Millipore	MAB 1281
Goat anti-pleiotrophin C-19	Santa Cruz Biotechnology	sc-1394
Goat anti-Sox2	R&D	AF2018
Rabbit glial fibrillary acidic protein	Stem Cell Technologies	60128
Rat myelin basic protein	Abcam	Ab7349
Alexa 594 donkey anti-goat IgG	Jackson ImmunoResearch	705-585-147
Alexa 405 donkey anti-mouse IgG	Jackson ImmunoResearch	715-475-151
Alexa 647 donkey anti-rabbit IgG	Jackson ImmunoResearch	711-605-152
Alexa 647 donkey anti-mouse IgG	Life Technologies	A-31571
Alexa 647 donkey anti-rat IgG	Jackson ImmunoResearch	712-605-150
Mouse anti-pleiotrophin H-6	Santa Cruz Biotechnology	sc-74443
Rabbit anti-SPARC	Santa Cruz Biotechnology	sc-390199
Mouse anti-SPARCL1	Santa Cruz Biotechnology	sc-25574
Rabbit anti-HSP90B	GeneTex	GTX101448
Rabbit normal IgG	Santa Cruz Biotechnology	sc-2027
Mouse normal IgG	Santa Cruz Biotechnology	sc-2025
Goat anti-SPARC	R&D	AF941
Goat anti-SPARCL1	R&D	AF2728
Rabbit anti-GRP78	Abcam	ab21685
Rabbit anti-PTPRZ	Thermo Fisher	PA5-51041
Rabbit beta-actin	Cell Signaling	4970S
Goat anti-rabbit IgG-HRP	Cell Signaling	7074S
Horse anti-mouse IgG-HRP	Cell Signaling	7076S
Donkey anti-goat IgG-HRP	Santa Cruz Biotechnology	sc-2020
Mouse anti-SPARC AON-1	Santa Cruz Biotechnology	sc-33645
Mouse anti-HSP90B H9010	Thermo Fisher	37-9400
Mouse anti-nestin clone 10C2	Millipore	MAB 5326
Rabbit anti-IGFBP2	Cell Signaling	3922S
Rabbit anti-brevican H-94	Santa Cruz Biotechnology	sc-292927
Alexa 488 donkey anti-mouse IgG	Jackson ImmunoResearch	711-545-152
Chemicals, Peptides, and Recombinant Proteins		
Human brevican	R&D	4009-BC-050
Human pleiotrophin	R&D	252-PL-050
Human SPARC	R&D	941-SP-050
Human SPARCL1	R&D	2728-SL-050
Human GRP78	Abcam	ab78432
Human HSP90B	Sigma-Aldrich	SRP0183
Human IGFBP2	PeproTech	350-06B
Human IGFBP4	PeproTech	350-05B
GSK 429286	Tocris	3726
GSK 269962A	A gift from Craig Thomas, NCATS	N/A

(*Continued on next page*)

Continued

REAGENT or RESOURCE	SOURCE	IDENTIFIER
17-AAG	SelleckChem	S1141
Critical Commercial Assays		
BioCoat growth factor reduced Matrigel invasion chambers	Corning	354483
Pierce Crosslink Magnetic IP/Co-IP kit	Thermo Scientific	88805
BCA protein assay	Thermo Scientific	23225
G-LISA RhoA absorbance-based activation assay	Cytoskeleton	BK124
Rho-associated kinase (ROCK) activity assay	Millipore	CSA001
CellTiter-Glo assay	Promega	G9242
Deposited Data		
Whole exome sequencing of SU-DIPG-XIII	This paper	EGAS00001002326
RNA sequencing of SU-DIPG-XIII	This paper	GSE99812
Raw data and statistics for non-sequencing data	This paper	http://dx.doi.org/10.17632/pbbsb6nx5f.1
Experimental Models: Cell Lines		
Human patient-derived high-grade glioma cell cultures; see Table S1	Venkatesh et al., 2015; Nagaraja et al., 2017; this paper	Table S1
CHL-1 melanoma cells	ATCC	ATCC CRL-9446
Experimental Models: Organisms/Strains		
Mouse: NOD-SCID-IL2R gamma chain-deficient (NSG)	The Jackson Laboratory	JAX: 005557
Mouse: C57BL/6J	The Jackson Laboratory	JAX: 000664
Mouse: CD1	The Jackson Laboratory	JAX: 022
Oligonucleotides		
Primer: mouse *Ptn* forward: 5′ CTCTGCACAATGCTGACTGTC 3′	PrimerBank	12857177a1
Primer: mouse *Ptn* reverse: 5′ CTTTGACTCCGCTTGAGGCTT 3′	PrimerBank	12857177a1
Primer: mouse *Actb* forward: 5′ GGCTGTATTCCCCTCCATCG 3′	PrimerBank	6671509a1
Primer: mouse *Actb* reverse: 5′ CCAGTTGGTAACAATGCCATGT 3′	PrimerBank	6671509a1
Primer: human *PTPRZ1* forward: 5′ GCTTTGATGCGGACCGATTTT 3′	PrimerBank	91208427c3
Primer: human *PTPRZ1* reverse: 5′ ACGACTAACACTTTCGACTCCA 3′	PrimerBank	91208427c3
Primer: human *ACTB* forward: 5′ CATGTACGTTGCTATCCAGGC 3′	PrimerBank	4501885a1
Primer: human *ACTB* reverse: 5′ CTCCTTAATGTCACGCACGAT 3′	PrimerBank	4501885a1
Human *PTN* shRNA: 5′ CCGGAGGC AAGAAACAGGAGAAGATCTCGAGA TCTTCTCCTGTTTCTTGCCTTTTTT 3′	Sigma	TRCN0000002774
Mouse *Ptn* shRNA: 5′ CCGGGCACAA TGCTGACTGTCAGAACTCGAGTTCT GACAGTCAGCATTGTGCTTTTTG 3′	Sigma	TRCN0000071676
Human *SPARC* shRNA: 5′ CCGGCCAGG TGGAAGTAGGAGAATTCTCGAGAATTCT CCTACTTCCACCTGGTTTTT 3′	Sigma	TRCN0000008711

(*Continued on next page*)

Continued

REAGENT or RESOURCE	SOURCE	IDENTIFIER
Human *SPARCL1* shRNA: 5′ CCGGATAC CCAATCTGATGATATTTCTCGAGAAATA TCATCAGATTGGGTATTTTTT 3′	Sigma	TRCN0000373631
Human *HSP90B1* shRNA: 5′ CCGGCCTG TGGATGAATACTGTATTCTCGAGAATAC AGTATTCATCCACAGGTTTTT 3′	Sigma	TRCN00000029425
Mouse *Hsp90b1* shRNA: 5′ CCGGGCTATT CAGTTGGATGGGTTACTCGAGTAACCCA TCCAACTGAATAGCTTTTTG 3′	Sigma	TRCN0000071925
Human *PTPRZ1* shRNA: 5′ CCGGATACCT AAGTCTTCGTTAATACTCGAGTATTAACG AAGACTTAGGTATTTTTT 3′	Sigma	TRCN0000356374
Scrambled shRNA: 5′ CCTAAGGTTAA GTCGCCCTCGCTCGAGCGAGGGCG ACTTAACCTTAGG 3′	Addgene	1864
Software and Algorithms		
Tophat2	Kim et al., 2013	https://ccb.jhu.edu/software/tophat/
featureCounts	Liao et al., 2014	http://bioinf.wehi.edu.au/featureCounts/
DESeq2	Love et al., 2014	https://bioconductor.org/packages/release/bioc/html/DESeq2.html
Gene Ontology Consortium	Ashburner et al., 2000	http://www.geneontology.org/

CONTACT FOR REAGENT AND RESOURCE SHARING

Further information and requests for resources and reagents should be directed to and will be fulfilled by the Lead Contact, Michelle Monje (mmonje@stanford.edu). SU cell cultures will be distributed through the Monje lab with a material transfer agreement (MTA) with Stanford University.

EXPERIMENTAL MODEL AND SUBJECT DETAILS

Mice and housing conditions

All animal procedures were approved by the Stanford University Administrative Panel on Laboratory Animal Care and performed in accordance with institutional and National Institutes of Health guidelines. All experiments were performed on NOD-SCID-IL2R gamma chain-deficient (NSG) or BL6/CD1 mice, with male and female animals used equally. Animals were housed according to standard guidelines with free access to food and water in a 12 hr light/dark cycle.

Patient-derived glioma cell culture

All human tissue studies were performed with informed consent and in accordance with Institutional Review Board (IRB)-approved protocols. Authenticity of all cultures was routinely monitored and validated using short tandem repeat (STR) DNA fingerprinting.

DIPG cell cultures were generated as tumor neurospheres from early post-mortem tissue as previously described (Caretti et al., 2014; Lin and Monje, 2017; Monje et al., 2011; Venkatesh et al., 2015). Briefly, tumor tissue was collected under sterile conditions, and transported in Hibernate-A (Thermo Scientific, Waltham, MA) on ice to the laboratory. The tissue was mechanically dissociated, followed by gentle rotation in enzymatic dissociation buffer (HEPES-HBSS with DNase I and liberase) at 37°C. Cells were then passed through a 100 μm cell strainer, and processed through a sucrose gradient to remove myelin. The resulting dissociated cells were treated with ACK lysis buffer (Thermo Scientific, Waltham, MA) to remove red blood cells, and plated in a serum-free medium designated "Tumor Stem Medium (TSM)," consisting of: Neurobasal (-A) (Invitrogen, Carlsbad, CA), B27 (-A) (Invitrogen, Carlsbad, CA), heparin (2 μg/mL; Stem Cell Technologies, Vancouver, BC, Canada), human-EGF (20 ng/mL; Shenandoah Biotech, Warwick, PA), human-bFGF (20 ng/mL; Shenandoah Biotech, Warwick, PA), PDGF-AA (10 ng/mL; Shenandoah Biotech, Warwick, PA), and PDGF-BB (10 ng/mL; Shenandoah Biotech, Warwick, PA).

The pediatric and adult glioblastoma cultures were obtained at the time of biopsy or autopsy, as indicated in Table S1, and were cultured and validated in the same way as for DIPG tissue described above.

The oligodendroglioma cultures were obtained at the time of biopsy, and generated similarly to the cultures described above and as previously described (Venkatesh et al., 2015). Briefly, the tissue was chopped finely, followed by gentle rotation in liberase at 37°C. Cells were triturated 8 times through a 10 mL serological pipette, followed by 8 times through a 1 mL pipette tip. The cells were then

passed through a 100 μm cell strainer, a sucrose gradient, and treated with ACK lysis buffer as described above. Cells were cultured in flasks coated with Matrigel (BD Biosciences, San Jose, CA).

All glioma cells described above were cultured in "Tumor Stem Medium (TSM)," a defined, serum-free medium described above.

Neural precursor cell culture and generation of conditioned medium

Human subventricular zone neural precursor cells were a generous gift from Siddhartha Mitra and Samuel Cheshier. The cells were cultured from the subventricular zone of the lateral ventricles (SVZ) from a 19-week fetus. Cells were cultured as a monolayer in human neural precursor cell medium (hNPC medium), consisting of: Neurobasal (-A) (Invitrogen, Carlsbad, CA), B27 (-A) or N2 (Invitrogen, Carlsbad, CA), heparin (2 μg/mL; Stem Cell Technologies, Vancouver, BC, Canada), human-EGF (20 ng/mL; Shenandoah Biotech, Warwick, PA), human-bFGF (20 ng/mL; Shenandoah Biotech, Warwick, PA), and human-LIF (20 ng/mL; Millipore, Bedford, MA).

Mouse neural precursor cells were cultured from WT BL6/CD1 mice at P14 as described by Walker and Kempermann (2014). The subventricular zone of the lateral ventricles, third ventricular zone, and fourth ventricular zone were microdissected. The tissue was minced and gently dissociated, passed through a 40 μm filter, and plated. Cells were cultured as a monolayer in mouse neural precursor cell medium (mNPC medium), consisting of: Neurobasal (-A) (Invitrogen, Carlsbad, CA), B27 (-A) or N2 (Invitrogen, Carlsbad, CA), heparin (2 μg/mL; Stem Cell Technologies, Vancouver, BC, Canada), mouse-EGF (20 ng/mL; Peprotech, Rocky Hill, NJ), and mouse-FGF-2 (20 ng/mL; Peprotech, Rocky Hill, NJ).

Conditioned medium was collected from mouse and human neural precursor cells at passage 5-10. Cells were grown in medium containing B27 (-A) for functional assays involving glioma cells, or in media containing N2 for proteomic and size exclusion chromatography analyses. After passaging, cells were plated in fresh NPC medium, and allowed to grow for 7 days, with addition of fresh medium on day 3-4. On day 7, cells were spun down, and the conditioned medium was collected and passed through a 0.22 μm filter. Conditioned medium was either used immediately or frozen at −80°C for future experiments.

Neuron culture and generation of conditioned medium

Mouse hippocampal neurons were cultured from WT BL6/CD1 mice at P0 as described by Beaudoin et al. (2012). The hippocampus was microdissected, minced, and gently dissociated. Cells were cultured in flasks coated with poly-L-lysine. Cells were plated initially in serum neuronal medium, consisting of: Minimal Essential Medium with Earle's salts (Invitrogen, Carlsbad, CA), glucose, and fetal bovine serum. All serum neuronal medium was removed after the first 4 hr, and cells were subsequently cultured in serum-free neurobasal medium, consisting of: Neurobasal (Invitrogen, Carlsbad, CA), B27 (Invitrogen, Carlsbad, CA), and Glutamax (Invitrogen, Carlsbad, CA). Serum-free neurobasal medium was refreshed every 3-4 days.

Conditioned medium was collected from mouse hippocampal neurons at 3 weeks after plating. At 2 weeks after plating, all medium was replaced with fresh serum-free neurobasal medium. Fresh medium was added after 3-4 days, and on day 7, the conditioned medium was collected and passed through a 0.22 μm filter. Conditioned medium was either used immediately or frozen at −80°C for future experiments.

Culture of CHL-1 melanoma cells

CHL-1 melanoma cells (ATCC, Manassas, VA) were cultured in "Tumor Stem Medium (TSM)," a defined, serum-free medium described above.

Orthotopic xenografting and lentiviral injections

NSG mice at age P34-36 were orthotopically xenografted with SU-DIPG-XIII frontal lobe CMV-GFP-luciferase cells, in a similar procedure to as previously described (Grasso et al., 2015; Venkatesh et al., 2015). Briefly, a single-cell suspension of SU-DIPG-XIII frontal lobe CMV-GFP-luciferase cells at passage 16-19 was prepared in sterile HBSS immediately before beginning the xenograft procedure. 600,000 cells in 3 μL were stereotactically injected into the pons of the left hemisphere of NSG mice, through a 31-gauge burr hole. Stereotactic coordinates used were: 1 mm lateral to midline, 0.8 mm posterior to lambda suture, and 5 mm deep. Cells were injected at a rate of 0.4 μL/min using a digital pump and a 31-gauge Hamilton syringe. After infusion of cells, the syringe needle was kept in place for 2 min, and then withdrawn manually at a rate of 0.875 mm/min to minimize the backflow of cells.

Mice used for shRNA lentivirus studies received shRNA-expressing lentivirus in the SVZ at P27-29 and DIPG cells in the left pons at P34-36. For lentiviral injections, 2 μL of shRNA-expressing lentivirus were stereotactically injected into the SVZ. Stereotactic coordinates used were: 1.3 mm lateral to midline, 0.1 mm posterior to bregma suture, and 2 mm deep. Virus was injected and the needle was withdrawn according to the same procedure as described above.

Human SVZ samples

All human tissue studies were performed with informed consent and in accordance with Institutional Review Board (IRB)-approved protocols. Human SVZ samples demonstrating PTN expression were obtained at autopsy from an 8-year-old female and a 68-year-old male. Human SVZ samples demonstrating glioma invasion were obtained at the time of autopsy from subjects described in Caretti et al., 2014 and in Table S1.

METHOD DETAILS

Bioluminescent IVIS imaging

Mice were imaged using an IVIS Spectrum to ensure tumor engraftment and monitor tumor size. Mice were anesthesized under 1% isoflurane, intraperitoneally injected with luciferin (15 mg/kg), and imaged for bioluminescence every minute until the peak total flux was reached.

Drug treatment of mice

Orthotopically xenografted mice that were treated with 17-AAG or a vehicle control received treatment from 1 week after xenograft until sacrifice. 17-AAG was freshly formulated immediately before injections at 10 mg/mL in 5% DMSO/ 95% corn oil. Mice received 50 mg/kg 17-AAG 5 days per week (5 days on, 2 days off). Vehicle-treated control mice received 5 uL/g 5% DMSO/ 95% corn oil on the same dosing schedule. Mice were perfused 8 weeks after xenograft.

Perfusion and immunohistochemistry

Mice were intraperitoneally injected with Avertin (tribromoethanol) for anesthesia, and then transcardially perfused with 20 mL of ice-cold PBS. Brains were dissected out and fixed in 4% paraformaldehyde in PBS overnight at 4°C, and were then transferred to 30% sucrose in PBS for cryoprotection. Brains were embedded in Tissue-Tek O.C.T. (Sakura, Torrance, CA). Brains from mice older than P10 were sliced into 40 μm coronal or sagittal sections using a sliding microtome (Microm HM450; Thermo Scientific, Waltham, MA). Brains from mice age P0 to P10 were sliced into 25 μm coronal sections using a cryostat (Leica Biosystems CM3050 S; Wetzlar, Germany). For immunohistochemistry, a 1 in 6 series of 25 μm or 40 μm sections was incubated in blocking solution (3% normal donkey serum, 0.3% Triton X-100 in TBS) at room temperature for 1 hr. Sections were incubated in primary antibodies diluted in 1% blocking solution (1% normal donkey serum, 0.3% Triton X-100 in TBS) overnight at 4°C, rinsed in TBS the following day, and then incubated in secondary antibodies diluted in 1% blocking solution overnight at 4°C. The following day, sections were rinsed and mounted using ProLong Gold mounting medium with or without DAPI (Life Technologies, Carlsbad, CA).

Primary antibodies used were: mouse anti-human nuclei clone 235-1 (1:100; Millipore, Bedford, MA), goat anti-pleiotrophin (1:250; Santa Cruz Biotechnology, Santa Cruz, CA), mouse anti-SPARC (1:100; Santa Cruz Biotechnology, Santa Cruz, CA), goat anti-SPARCL1 (1:100; R&D Systems, Minneapolis, MN), mouse anti-HSP90B (1:100; Thermo Fisher, Waltham, MA), mouse anti-nestin (1:250; Millipore, Bedford, MA), goat anti-Sox2 (1:50; R&D Systems, Minneapolis, MN), rabbit glial fibrillary acidic protein (1:200; Stem Cell Technologies, Vancouver, Canada), and rat myelin basic protein (1:200; Abcam, Cambridge, MA).

Secondary antibodies used were: Alexa 594 donkey anti-goat IgG (1:500; Jackson ImmunoResearch, West Grove, PA), Alexa 405 donkey anti-mouse IgG (1:500; Jackson ImmunoResearch, West Grove, PA), Alexa 488 donkey-anti-mouse IgG (1:500; Jackson ImmunoResearch, West Grove, PA), Alexa 647 donkey-anti-rabbit IgG (1:500; Jackson ImmunoResearch, West Grove, PA), Alexa 647 donkey anti-mouse IgG (1:500; Life Technologies, Carlsbad, CA), and Alexa 647 donkey anti-rat IgG (1:500; Jackson ImmunoResearch, West Grove, PA).

Analysis of tumor spread over time

For analysis of DIPG spread in the mouse brain over time, 25 mice were orthotopically xenografted as described above. 8 mice were sacrificed at 4 weeks post-xenograft, 8 mice were sacrificed at 8 weeks post-xenograft, and 9 mice were sacrificed at 16 weeks post-xenograft. A 1:6 series of sagittal slices was stained and imaged, and the anatomical locations of GFP^+ HNA^+ cells throughout each mouse were noted and compared with the Allen Brain Atlas.

Matrigel invasion assay

To test for chemoattraction and invasion toward neural precursor cell conditioned medium or another candidate chemoattractant, a single-cell suspension of 100,000 tumor cells in Tumor Stem Medium (TSM) base (with B27 (-A) and heparin, without growth factors) was seeded in the top inserts of BioCoat growth factor reduced Matrigel invasion chambers (Corning, Bedford, MA), after rehydration of the inserts. Chemoattractant medium was added to the bottom of the chamber. All conditions were plated in triplicate. After 72 hr, medium was aspirated, and the non-invading cells on top of the layer of Matrigel were scrubbed off. The invading cells were fixed in 4% paraformaldehyde and then stained with 0.1% crystal violet in 10% methanol in distilled water. The number of invading cells was quantified by the intensity of the crystal violet dye on the invading side of the Matrigel. The dye was collected in 10% acetic acid, and absorbance was measured at 595 nm.

To test for phenotypic change induced by direct exposure to neural precursor cell conditioned medium, 100,000 DIPG cells were seeded in the top inserts of the Matrigel invasion assay in conditioned medium, and TSM base (with B27 (-A) and heparin) was plated in the bottom chambers. The rest of the procedure was performed as described above.

To test the ROCK or HSP90 inhibitors in the Matrigel invasion assay, the inhibitors were added to the suspension of glioma cells in TSM base (with B27 (-A) and heparin) seeded in the top inserts at the appropriate concentrations, and neural precursor cell conditioned medium was plated in the bottom chambers. The rest of the procedure was performed as described above.

Biochemical assays

For protein denaturation, medium samples were boiled for 7 min at 100°C. For RNA and DNA degradation, medium samples were treated with RNase and/or DNase at 2 μg/mL for one hour. For size fractionation, medium samples were spun in 30 kDa Amicon ultracentrifugal filters (Millipore, Bedford, MA), and volumes were normalized by addition of fresh unconditioned NPC medium. All experiments were performed in triplicate.

Two-dimensional gel electrophoresis

Two-dimensional gel electrophoresis (2-D DIGE) and the subsequent protein identification processes were performed by Applied Biomics, Inc (Hayward, CA), as previously described (Venkatesh et al., 2015). The procedure is summarized in brief below.

Sample preparation and CyDye labeling

Protein sample buffer was exchanged into 2-D cell lysis buffer (30 nM Tris-HCl, pH 8.8, containing 7 M urea, 2 M thiourea, and 4% CHAPS), and protein concentration was measured by the Bio-Rad protein assay method (Hercules, CA). Proteins were labeled with CyDye, and the labeled samples were mixed together. The 2x 2-D sample buffer (8 M urea, 4% CHAPS, 20 mg/mL DTT, 2% pharmalytes, and trace amount of bromophenol blue), 100 μL destreak solution and rehydration buffer (7 M urea, 2 M thiourea, 4% CHAPS, 20 mg/mL DTT, 1% pharmalytes, and trace amount of bromophenol blue) were added to the labeling mix.

IEF and SDS-PAGE

After loading the labeled samples, IEF (pH 3-10) was run according to the GE Healthcare protocol. The IPG strips were incubated in fresh equilibration buffer-1 (50 mM Tris-HCl, pH 8.8, containing 6 M urea, 30% glycerol, 2% SDS, trace amount of bromophenol blue and 10mg/mL DTT), and subsequently rinsed in fresh equilibration buffer-2 (50 mM Tris-HCl, pH 8.8, containing 6 M urea, 30% glycerol, 2% SDS, trace amount of bromophenol blue, and 45 mg/mL Iodoacetamide) and SDS-gel running buffer. The strips were transferred into 12% SDS-gels, which were run at 15°C until the dye front ran out of the gels.

Image Scan and Analysis

Immediately after SDS-PAGE, gel images were scanned using Typhoon TRIO (GE Healthcare, Waukesha, WI). The images were analyzed by Image Quant software (version 6.0, GE Healthcare, Waukesha, WI), and quantitation analysis was done with DeCyder software (version 6.5, GE Healthcare, Waukesha, WI). In-gel DeCyder analysis was used to obtain the fold change of protein expression levels.

Protein identification by mass spectrometry

Spot picking and trypsin digestion

Based on the in-gel analysis and spot picking design by DeCyder software, spots of interest were picked up by Ettan Spot Picker (Amersham BioSciences, Piscataway, NJ). The gel spots were washed and digested with modified porcine trypsin protease (Trypsin Gold, Promega, Madison, WI). The digested tryptic peptides were desalted using Zip-tip C18 (Millipore, Bedford, MA), and the peptides were eluted using matrix solution (α-cyano-4-hydroxycinnamic acid 5 mg/mL in 50% acetonitrile, 0.1% trifluoroacetic acid, 25 mM ammonium bicarbonate) and spotted on the AB SCIEX MALDI plate (Opti-TOF 384 Well Insert, AB SCIEX, Framingham, MA).

Mass spectrometry

MALDI-TOF MS and TOF/TOF tandem MS/MS were performed using an AB SCIEX TOF/TOF 5800 System (AB SCIEX, Framingham, MA). In reflectron positive ion mode, MALDI-TOF mass spectra were acquired, with an average of 4000 laser shots per spectrum. For each sample, TOF/TOF tandem MS fragmentation spectra were acquired, with an average of 4000 laser shots per fragmentation spectrum on each of the 10 most abundant ions in each sample (excluding known background ions such as trypsin autolytic peptides).

Database search

The resulting peptide mass and associated fragmentation spectra were submitted to search the Swiss-Prot database via a GPS Explorer workstation equipped with MASCOT search engine (Matrix Science, Boston, MA). Searches were performed with no constraining protein molecular weight or isoelectric point, with variable oxidation of methionine and carbamidomethylation of cysteine residues, and with one missed cleavage allowed. Candidates with either ion C.I.% or protein score C.I.% greater than 95 were considered significant.

Recombinant proteins used

BCAN, PTN, SPARC, SPARCL1 (R&D Systems, Minneapolis, MN), GRP78 (Abcam, Cambridge, MA), HSP90B (Sigma-Aldrich, St. Louis, MO), IGFBP2, and IGFBP4 (PeproTech, Rocky Hill, NJ).

Size exclusion chromatography

Human SVZ neural precursor cell conditioned medium was concentrated to 5 mg/mL using 3 kDa Amicon ultracentrifugal filters (Millipore, Bedford, MA), and subsequently centrifuged at 21,000 x g for 10 min. Prior to running the sample, the column was calibrated with size standards using the Gel Filtration High Molecular Weight Calibration Kit (GE Healthcare, Waukesha, WI) to ensure proper calibration. 500 μL of conditioned medium was fractionated on a Superose 6 10/300 GL column (GE Healthcare, Waukesha, WI) via elution with 1.5 column volumes of gel filtration buffer (25 mM HEPES [pH 7.5], 150 mM NaCl, 1 mM DTT) at a flow rate of

0.25 mL/min and collecting 250 μL fractions. Each fraction was then analyzed by immunoblotting. The approximate molecular weights of the eluted proteins were determined by comparing with proteins of known molecular weight (Gel Filtration Calibration Kit; GE Healthcare, Waukesha, WI).

Immunoprecipitation

Immunoprecipitation reactions were conducted using the Pierce Crosslink Magnetic IP/Co-IP Kit (Thermo Scientific, Waltham, MA). 25 μL of Pierce Protein A/G Magnetic Beads per reaction were rinsed and incubated with 5 μg of antibody on a rotating platform for 15 min at room temperature. Antibodies used were: mouse anti-pleiotrophin (Santa Cruz Biotechnology, Santa Cruz, CA), rabbit anti-SPARC (Santa Cruz Biotechnology, Santa Cruz, CA), mouse anti-SPARCL1 (Santa Cruz Biotechnology, Santa Cruz, CA), rabbit anti-HSP90B (GeneTex, Irvine, CA), rabbit normal IgG (Santa Cruz Biotechnology, Santa Cruz, CA), and mouse normal IgG (Santa Cruz Biotechnology, Santa Cruz, CA). Beads were rinsed, and subsequently crosslinked to the antibodies using 0.02 mM DSS for 30 min at room temperature. Beads were washed and then incubated with a mixed combination of 250 μL neural precursor cell conditioned medium and 250 μL IP lysis/wash buffer overnight at 4°C. The following morning, beads were washed, resuspended in Laemmli loading buffer, and boiled at 100°C for 5 min to release the bound antigens from the beads. Samples were loaded immediately onto western blots for analysis of the bound antigens, or stored at −20°C for future analysis. For western blot analysis, 2% of the input conditioned medium was loaded, and 5% of the IP bound antigen samples were loaded.

For immunodepletion reactions, 100 μL of beads and 20 μg of antibody were used per reaction. Beads were incubated overnight with pure conditioned medium, and subsequently, the beads as well as the unbound sample (the depleted conditioned medium) were collected. The depleted conditioned medium was used immediately in the Matrigel invasion assay, with an aliquot set aside for confirmation of depletion by western blot. The rest of the procedure was performed as described above.

Western blot analysis

Conditioned medium samples were mixed with Laemmli loading buffer (1:4) and boiled for 5 min at 100°C. Cells or tissue samples were lysed in RIPA buffer and protease inhibitors, incubated on ice for 30 min, and centrifuged for 15 min at 15,000 rpm at 4°C. Protein concentration in the lysates was determined using the BCA protein assay (Thermo Scientific, Waltham, MA). The protein concentration of the samples was normalized, and samples were mixed with Laemmli loading buffer (1:4) and boiled for 5 min at 100°C.

Samples were run on Bio-Rad Mini-Protean TGX precast gels (Bio-Rad, Hercules, CA), and the protein was transferred onto polyvinylidene fluoride (PVDF) membranes. Membranes were blocked with 5% bovine serum albumin (BSA) in TBST for 1 hr, and incubated in primary antibodies diluted in 1% BSA/TBST overnight at 4°C. Primary antibodies used were: mouse anti-pleiotrophin (1:100; Santa Cruz Biotechnology, Santa Cruz, CA), goat anti-SPARC (1:100; R&D Systems, Minneapolis, MN), goat anti-SPARCL1 (1:000; R&D Systems, Minneapolis, MN), rabbit anti-HSP90B (GeneTex, Irvine, CA), rabbit anti-GRP78 (1:500, Abcam, Cambridge, MA), rabbit anti-PTPRZ (1:2000; Thermo Fisher, Waltham, MA), and rabbit beta-actin (1:2000; Cell Signaling, Danvers, MA). Secondary antibodies conjugated to horseradish peroxidase (HRP) were added for 1 hr at room temperature (1:1000). Secondary antibodies used were: goat anti-rabbit IgG-HRP (Cell Signaling, Danvers, MA), horse anti-mouse IgG-HRP (Cell Signaling, Danvers, MA), and donkey anti-goat IgG-HRP (Santa Cruz Biotechnology, Santa Cruz, CA). Proteins were visualized using Clarity Western ECL Substrate (Bio-Rad, Hercules, CA).

Dissection of mouse SVZ and cortex

The SVZ and cortex were microdissected from P42 WT Bl6/CD1 mice for RNA and protein analyses. The SVZ was microdissected as described in Walker and Kempermann (2014), and a piece of lateral cortex was taken far from the SVZ. Tissue samples were immediately homogenized in TRIzol Reagent for RNA extraction or in RIPA buffer for protein extraction.

qPCR

Cells or tissue were lysed and homogenized in TRIzol Reagent (Life Technologies, Carlsbad, CA) and RNA was extracted according to reagent protocol. RNA was treated with dsDNase, and cDNA was synthesized using Thermo Scientific Maxima First Strand cDNA Synthesis Kit for RT-qPCR with dsDNase (Thermo Fisher Scientific K1671). RT-PCR was performed on Eppendorf Mastercycler Realplex2 using Universal SYBR Green Supermix (BioRad, Hercules, CA). Differential expression was determined using the deltaCt method. Primers used were as follows:

Mouse *Ptn* forward: 5′ CTCTGCACAATGCTGACTGTC 3′; mouse *Ptn* reverse 5′ CTTTGACTCCGCTTGAGGCTT 3′; mouse *Actb* forward: 5′ GGCTGTATTCCCCTCCATCG 3′; mouse *Actb* reverse: 5′ CCAGTTGGTAACAATGCCATGT 3′; human *PTPRZ1* forward: 5′ GCTTTGATGCGGACCGATTTT 3′; human *PTPRZ1* reverse: 5′ ACGACTAACACTTTCGACTCCA 3′; human *ACTB* forward: 5′ CATGTACGTTGCTATCCAGGC 3′; human *ACTB* reverse: 5′ CTCCTTAATGTCACGCACGAT 3′.

shRNA-expressing lentivirus preparation and infection

shRNA constructs against human and mouse PTN, human SPARC, human SPARCL1, human and mouse HSP90B1, and human PTPRZ1 from the RNAi consortium human collection were purchased from Sigma (St. Louis, MO). Scrambled shRNA was a gift

from David Sabatini (Addgene plasmid #1864). 293T cells were co-transfected with the shRNA constructs and packaging plasmids (pDelta 8.92 + VSV-G) to generate lentiviral particles. Lentiviral particles were concentrated using the polyethylene glycol (PEG) precipitation method, resuspended in PBS, and stored at −80°C.

For lentiviral infection, DIPG cells or neural precursor cells were exposed to shRNA-expressing lentivirus for 48 hr. Puromycin was added 48 hr after infection to select for virally infected cells. After removal of puromycin, shRNA-treated neural precursor cells were grown for 7 days (with addition of medium on day 3-4) for generation of conditioned medium. After removal of puromycin, shRNA-treated DIPG cells were grown for at least one passage before experimental use. shRNA construct sequences were as follows: Human *PTN* shRNA: 5′ CCGGAGGCAAGAAACAGGAGAAGATCTCGAGATCTTCTCCTGTTTCTTGCCTTTTTT 3′; Mouse *Ptn* shRNA: 5′ CCGGGCACAATGCTGACTGTCAGAACTCGAGTTCTGACAGTCAGCATTGTGCTTTTTG 3′; Human *SPARC* shRNA: 5′ CCGGCC AGGTGGAAGTAGGAGAATTCTCGAGAATTCTCCTACTTCCACCTGGTTTTT 3′; Human *SPARCL1* shRNA: 5′ CCGGATACCCAAT CTGATGATATTTCTCGAGAAATATCATCAGATTGGGTATTTTTT 3′; Human *HSP90B1* shRNA: 5′ CCGGCCTGTGGATGAATACTG TATTCTCGAGAATACAGTATTCATCCACAGGTTTTT 3′; Mouse *Hsp90b1* shRNA: 5′ CCGGGCTATTCAGTTGGATGGGTTACTCG AGTAACCCATCCAACTGAATAGCTTTTTG 3′; Human *PTPRZ1* shRNA: 5′ CCGGATACCTAAGTCTTCGTTAATACTCGAGTATTAAC GAAGACTTAGGTATTTTTT 3′; Scrambled shRNA: 5′ CCTAAGGTTAAGTCGCCCTCGCTCGAGCGAGGGCGACTTAACCTTAGG 3′.

RhoA and ROCK activation assays

SU-DIPG-XIII frontal lobe cells were starved in TSM base (without B27 (-A) supplement, heparin, or growth factors) for 48 hr prior to treatment. After treatment, cells were lysed in the RhoA activation assay kit cell lysis buffer (Cytoskeleton, Denver, CO). Lysates were incubated on ice for 1 min, clarified by centrifugation at 10,000 x g, 4°C for 1 min, and the supernatants were snap-frozen and stored immediately at −80°C. Protein concentrations were measured by the BCA protein assay (Thermo Scientific, Waltham, MA), and samples were diluted to 0.5 mg/mL by the addition of cell lysis buffer.

RhoA activation assays were performed using the G-LISA RhoA absorbance-based activation assay (Cytoskeleton, Denver, CO). Lysate samples were incubated in a 96-well plate with pre-linked Rho GTP-binding protein for 30 min at 4°C shaking at 400 rpm. Wells were incubated in anti-RhoA primary antibody (1:250) at room temperature for 45 min shaking at 400 rpm. Secondary HRP-labeled antibody (1:62.5) was added at room temperature for 45 min shaking at 400 rpm. Results were visualized by addition of HRP detection reagents for 12 min at 37°C, and the absorbance was read at 490 nm. All assays were performed in triplicate.

ROCK activation assays were performed using the Rho-associated kinase (ROCK) activity assay (Millipore, Bedford, MA). Cell lysates were incubated in wells of a myosin phosphatase target subunit 1 (MYPT1) pre-coated 96-well plate, for 30 min at 30°C with moderate shaking. Wells were incubated in anti-phospho-MYPT1(Thr696) primary antibody (1:1000) for 1 hr with moderate shaking. Goat anti-rabbit IgG HRP secondary antibody (1:2000) was added for 1 hr with moderate shaking. Results were visualized with TMB/E substrate, incubating in the dark for 10 min, and absorbance was read at 450 nm. All assays were performed in triplicate.

Pharmacologic inhibition

DIPG cells were treated with a dose curve of GSK 429286 (Tocris, Bristol, United Kingdom), GSK 269962A (a kind gift from Craig Thomas, National Center for Advancing Translational Sciences), or 17-AAG (SelleckChem, Houston, TX). All experiments using pharmacologic inhibitors used vehicle DMSO as a control.

Whole exome sequencing

Samples underwent sequencing on an Illumina HiSeq 2500 using Agilent's v6 SureSelect whole exome capture set. Short read sequences from whole exome or whole genome sequencing were aligned to the hg19 assembly of the human genome using bwa. Following duplicate removal with Picard tools variants were called using the Genome Analysis toolkit according to standard Best Practices (Broad) including local re-alignment around Indels, downsampling and variant calling with the Unified Genotyper. Variants were annotated with the variant Effect predictor v74 from Ensembl tools and ANNOVAR to include annotations for variant allele frequency in 1000 genomes dbSNP v 132 and the ExAc database as well as functional annotation tools SIFT and PolyPhen.

Coverage of aligned reads was binned into known exons with BEDTools and $\log_2$ ratios of median coverage in tumor and normal sequences were processed with in-house scripts. CBS binary segmentation was applied to each dataset to provide smoothed $\log_2$ ratios. Genes within common CNVs in normal individuals were excluded from further analysis with reference to the CNV map of the human genome. Exon-level median log ratios and smoothed values were thresholded to call gains and losses above and below $\log_2$ ratios of ± 0.3 with a contig of ~1MB and amplifications and deletions above and below a threshold of ± 1.5 with a minimum of 3 contiguous exons.

The accession number for whole exome sequencing data deposited in The European Genome-phenome Archive (EGA) database is EGA: EGAS00001002326.

RNA sequencing

RNA sequencing was performed as previously described (Nagaraja et al., 2017). Cells were lysed in TRIzol Reagent (Life Technologies, Carlsbad, CA) and RNA was extracted according to reagent protocol. 2 μg of total RNA was used for poly(A)$^+$ purification using Dynabeads mRNA Purification Kit (Thermo Fisher Scientific 61006). mRNA was fragmented using RNA Fragmentation Reagent (Ambion AM8740) and purified using ethanol precipitation. First strand synthesis was performed with SuperScript II (Invitrogen

18064-014) followed by second strand synthesis using DNA Polymerase I (Invitrogen 18010-025) and RNaseH (Invitrogen 18021-014). cDNA was purified using MinElute PCR Purification Kit (QIAGEN 28606).

Purified cDNA was end-repaired using T4 polymerase, Klenow fragment, and T4 PNK and then A-tailed using (exo-) Klenow. NEBNext Multiplex Oligo adaptors (New England BioLabs, E7335S) were ligated using Quick Ligation Kit (New England Biolabs, M2200L) overnight at RT. Adaptors were cut using USER Enzyme and adaptor-ligated libraries were purified by agarose gel electrophoresis. Libraries were amplified using NEBNext Multiplex Oligo primers and final libraries were purified using Ampure XP beads. Sequencing was performed on an Illumina NextSeq by Stanford Functional Genomics Facility.

Reads were aligned to the hg19 genome using tophat2 (Kim et al., 2013). Transcript abundance was calculated using featureCounts against a RefSeq gene annotation (Liao et al., 2014). Differential testing was done using DESeq2 with default median normalization (Love et al., 2014). Gene Ontology on upregulated genes was performed using Gene Ontology Consortium (Ashburner et al., 2000). Volcano plot was made in R.

RNA sequencing data are deposited in the GEO database. Accession number GEO: GSE99812.

CellTiter-Glo assay

To assess cell viability, 5,000 DIPG cells per well were seeded in base medium or conditioned medium in a 96-well plate. Inhibitors were added at the appropriate concentrations. After 72 hr, CellTiter-Glo reagent 2.0 (Promega, Madison, WI) was added at a 1:1 ratio, and cells were lysed. Luminescence was measured after stabilization of signal for 10 min at room temperature.

QUANTIFICATION AND STATISTICAL ANALYSIS

Stereological cell counting

For quantification of DIPG invasion of the SVZ after knock down of targets in the SVZ, 5 NSG mice per group were injected with shRNA-expressing lentivirus in bilateral SVZs and orthotopically xenografted with SU-DIPG-XIII FL in the left pons. Mice were perfused for analysis 16 weeks after xenograft. A 1:6 series of coronal slices from each mouse brain was immunostained and imaged, and the number of GFP^+ HNA^+ glioma cells within 200 μm of the lateral ventricles in all slices containing lateral ventricles was manually counted.

For quantification of DIPG invasion of the SVZ in mice xenografted with *PTPRZ1* knock down DIPG cells or scrambled shRNA control cells, or in mice treated with 17-AAG or vehicle control, 8 NSG mice per group were orthotopically xenografted in the left pons. Mice were perfused for analysis 8 weeks after xenograft. A 1:6 series of coronal slices from each mouse brain was immunostained and imaged, and the number of GFP^+ HNA^+ glioma cells within 200 μm of the left lateral ventricle in all slices containing lateral ventricles was manually counted.

For quantification of neural precursor cells in the SVZ after knock down of targets in the SVZ, a 1:6 series of coronal slices from each mouse was immunostained and imaged, and the number of $Sox2^+$ neural precursor cells in a 20x z stack was manually counted. The density of $Sox2^+$ cells was calculated as cells/mm^3.

Statistical analyses

All statistical analyses were performed using GraphPad Prism. The Shapiro-Wilk normality test was used to confirm Gaussian distribution for parametric analyses. For parametric datasets, unpaired two-tailed Student's t tests were used for comparisons between two samples, and group mean differences between more than two samples were assessed using one-way analysis of variance (one-way ANOVA) with Tukey or Dunnett post hoc tests to adjust for multiple comparisons. For nonparametric datasets, unpaired two-tailed Mann-Whitney tests were used for comparison between two samples. A level of $p < 0.05$ was used to determine significant differences.

DATA AND SOFTWARE AVAILABILITY

Patient-derived cell cultures

All patient-derived glioma cell cultures can be obtained through the Monje Lab with a materials transfer agreement with Stanford University. Contact Michelle Monje (mmonje@stanford.edu).

Sequencing data

The accession numbers for all DNA and RNA sequence data reported in this paper are EGA: EGAS00001002326 and GEO: GSE99812.

Raw data and statistics

Raw data and statistics for all non-sequencing data are available through Mendeley Data: http://dx.doi.org/10.17632/pbbsb6nx5f.1.

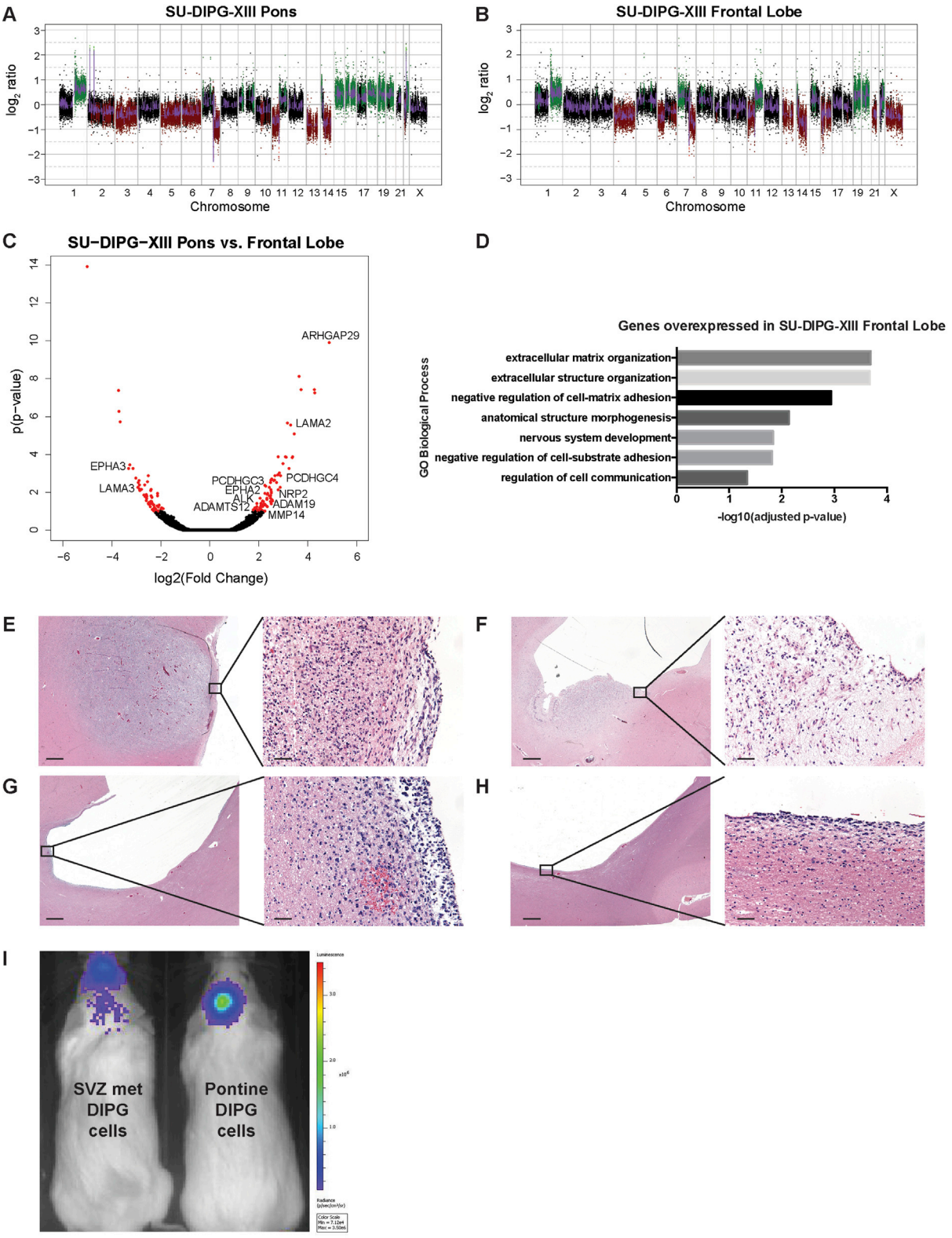

Figure S1. Characterization of Pontine and SVZ DIPG Cells, Related to Figure 1

(A and B) Copy-number plots of whole exome sequencing of DIPG cells isolated from the pons (A) and from an SVZ site of spread (B) from the same individual (SU-DIPG-XIII).

(legend continued on next page)

(C) Volcano plot of RNA sequencing comparing DIPG cells isolated from the pons and from an SVZ site of spread from SU-DIPG-XIII. x axis represents log2(fold change) of frontal lobe over pons; y axis shows -log10(Benjamini-Hochberg adjusted p value) from differential testing. Points in red represent those with adjusted p values less than 0.1.

(D) GO biological processes significantly overexpressed in the frontal lobe compared to the pontine culture of SU-DIPG-XIII. p values shown are Bonferroni adjusted.

(E–H) H&E of tumor in the lateral wall of the lateral ventricle SVZ in SU-DIPG-XVII (E), SU-DIPG-III (F), and SU-DIPG-VI (G and H). Low-magnification images are shown in the left panels: scale bar, 1 mm. High-magnification images are shown in the right panels: scale bar, 50 μm.

(I) Pontine DIPG cells are found primarily in the hindbrain in orthotopic xenografts by bioluminescent IVIS imaging, compared to SVZ DIPG cells, which are found in the forebrain and hindbrain.

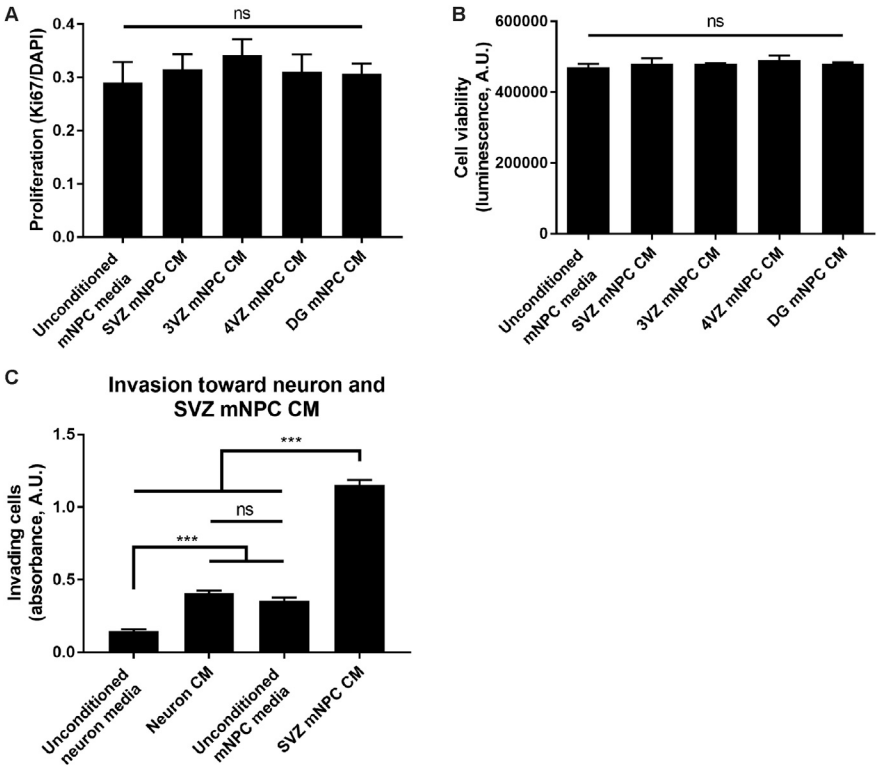

Figure S2. mNPC CM Has No Effect on DIPG Cell Proliferation or Viability, Related to Figure 2

(A) Cell proliferation of DIPG cells (fraction of $Ki67^+$ cells) when exposed to unconditioned or conditioned mNPC medium.

(B) Cell viability of DIPG cells by the CellTiter-Glo assay when exposed to unconditioned or conditioned mNPC medium.

(C) DIPG cells invade less toward murine neuron conditioned medium compared to SVZ mNPC CM.

All experiments performed with n = 3 replicates/wells (A, C) or n = 4 replicates/wells (B) in SU-DIPG-XIII FL cells and analyzed by one-way ANOVA with Tukey post hoc adjustment for multiple comparisons. Data shown as mean ± SEM. ***$p < 0.001$.

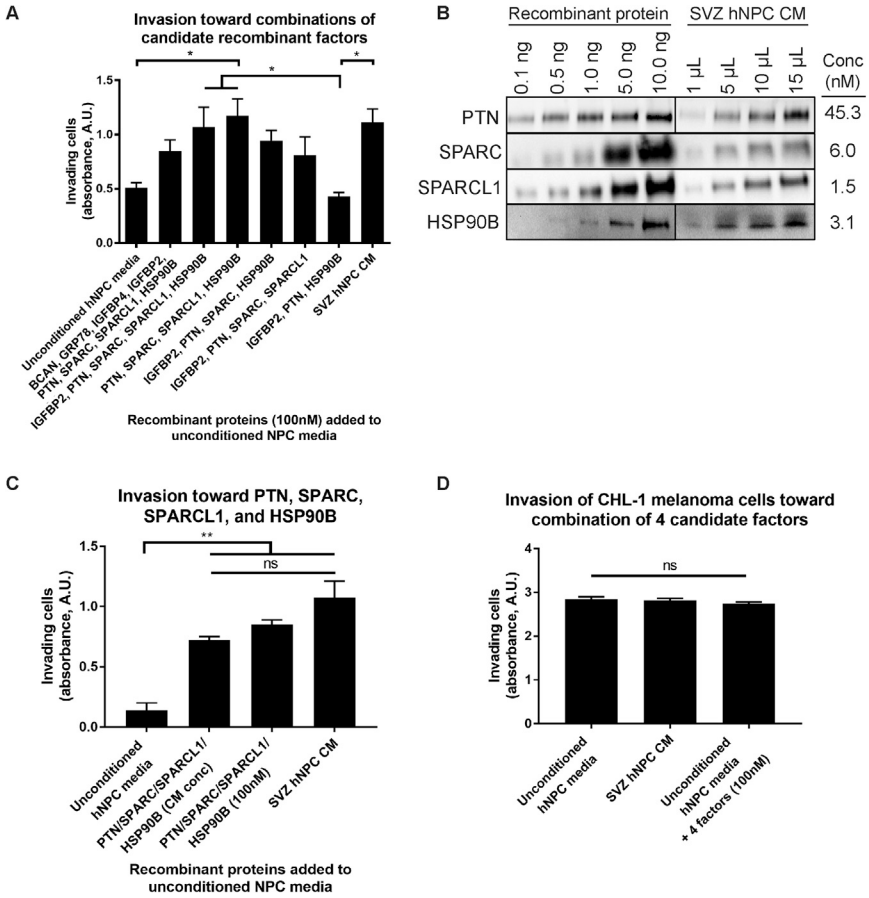

Figure S3. Invasion of DIPG Cells toward Candidate Recombinant Proteins, Related to Figure 4

(A) DIPG cells invade differentially toward various combinations of the eight candidate recombinant proteins. The combination of PTN, SPARC, SPARCL1, and HSP90B most closely replicates the invasion-promoting effect toward SVZ hNPC CM.

(B) Estimation of the concentration of PTN, SPARC, SPARCL1, and HSP90B in SVZ hNPC CM by western blot and ImageJ analyses. Vertical lines demarcate separate gels placed side-by-side in image in top and bottom rows, middle two rows each represent a single gel.

(C) The combination of PTN, SPARC, SPARCL1, and HSP90B is sufficient for DIPG invasion at 100nM as well as with each factor at its estimated concentration in the conditioned medium.

(D) CHL-1 melanoma cells invade similarly toward unconditioned hNPC medium, SVZ hNPC CM, and the combination of PTN, SPARC, SPARCL1, and HSP90B. Experiments performed with n = 3 replicates/wells in SU-DIPG-XIII FL cells (A, C) or in CHL-1 melanoma cells (D) and analyzed by one-way ANOVA with Tukey post hoc adjustment for multiple comparisons. Data shown as mean ± SEM. *$p < 0.05$, **$p < 0.01$.

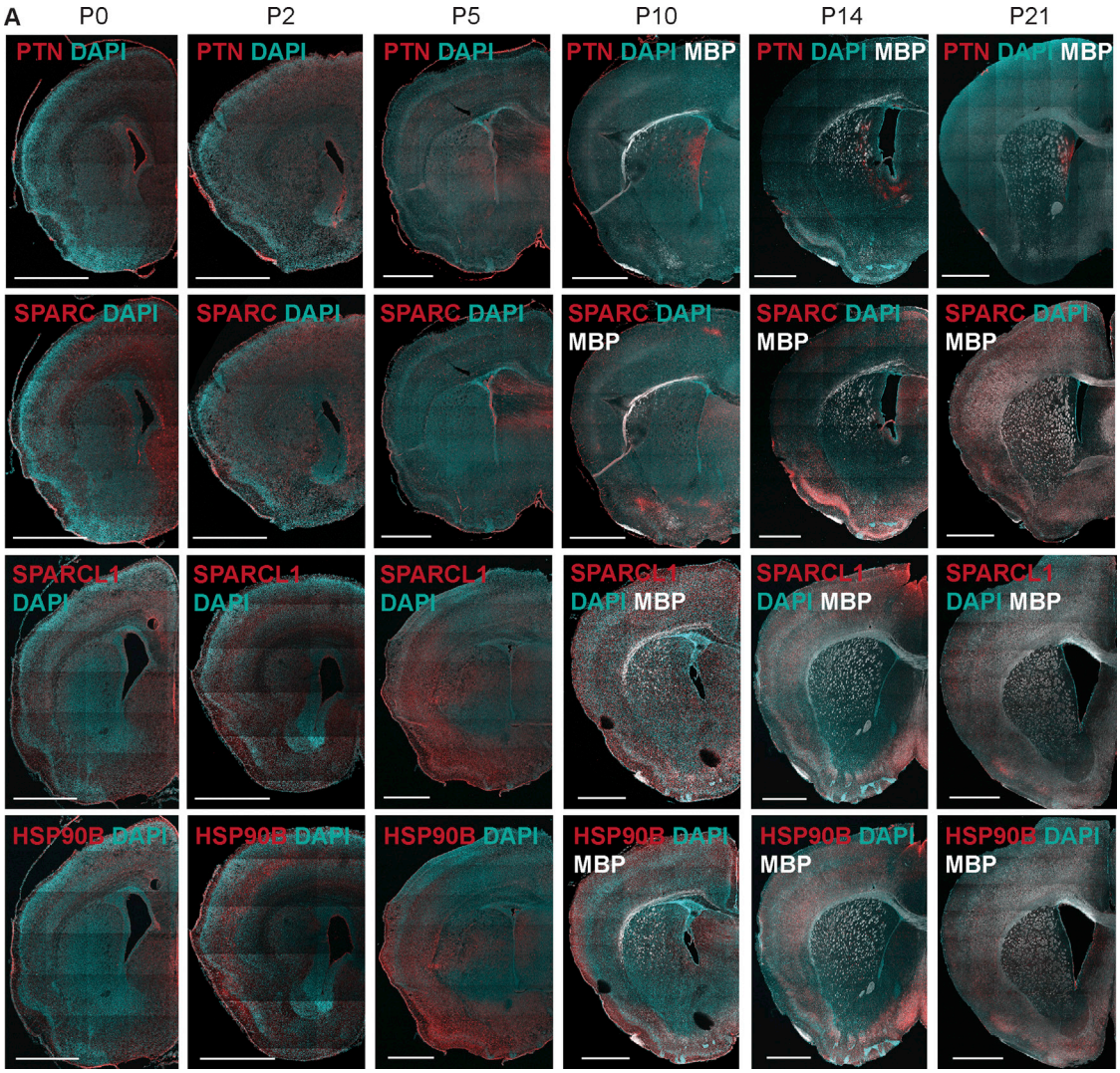

Figure S4. Expression of PTN and Its Binding Partners, Related to Figure 5

(A) Expression of PTN, SPARC, SPARCL1, and HSP90B in the forebrain at the level of the lateral ventricles in postnatal mice ages P0, 2, 5, 10, 14, and 21. PTN is more broadly expressed in the forebrain in P0-P5 mice, and becomes more restricted to the SVZ by P10. PTN is also expressed in the pia mater. SPARC, SPARCL1, and HSP90B are more broadly expressed in the brain.

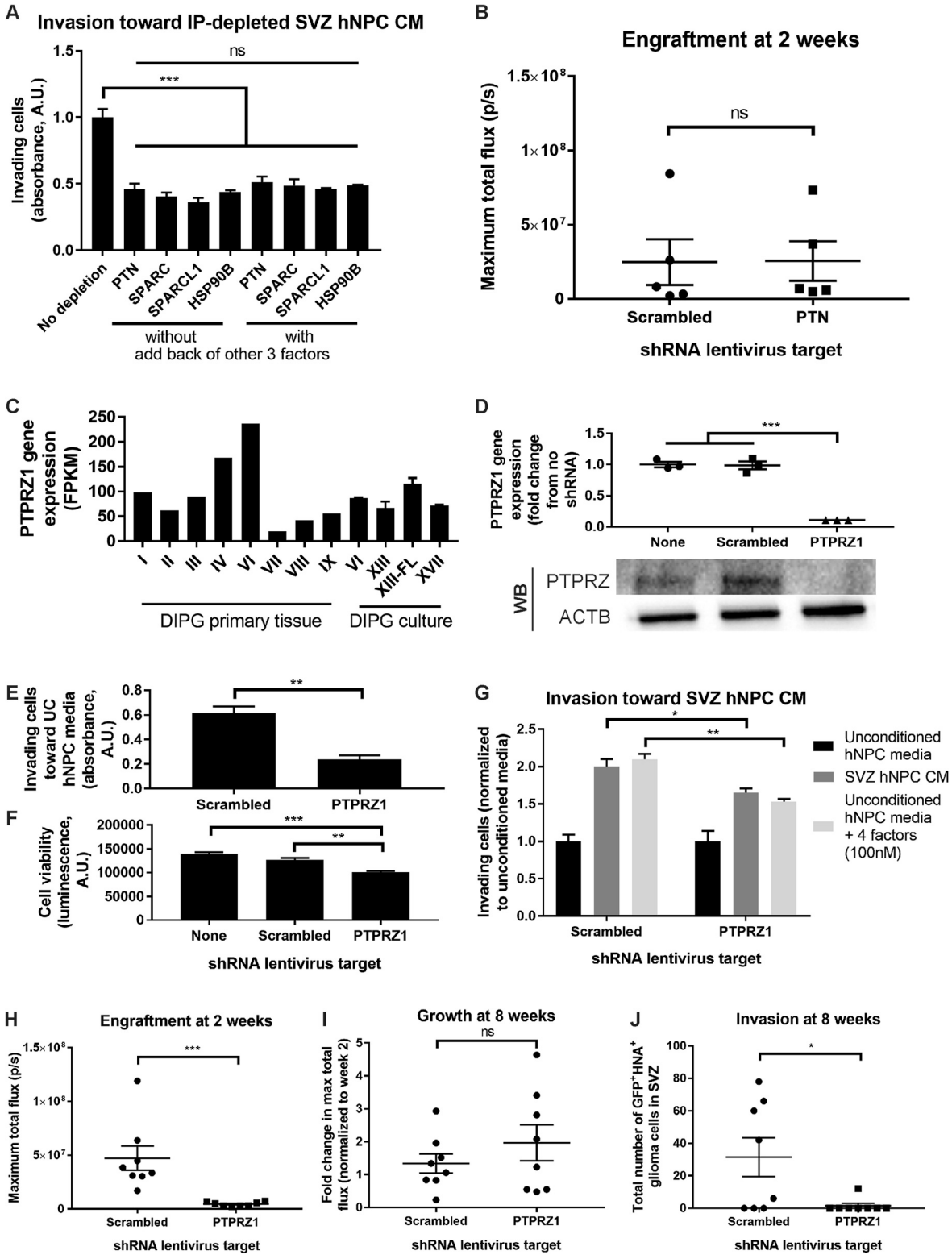

Figure S5. Necessity of PTN or PTPRZ, Related to Figure 6

(A) DIPG cells invade less toward SVZ hNPC CM after immunodepletion of any one of the four proteins, with or without add back of the other three proteins. Depletion of target proteins was confirmed by western blot (see Figure 6A). n = 3 replicates/wells in SU-DIPG-XIII FL cells and analyzed by one-way ANOVA with Tukey post hoc adjustment for multiple comparisons.

(legend continued on next page)

(B) Tumor engraftment was equivalent in mice that received injections of shRNA lentivirus targeting *Ptn* into the SVZ, compared to a scrambled shRNA control. In vivo experiments were performed with n = 5 mice per group. Bioluminescent flux measurements were analyzed by unpaired, two-tailed Mann-Whitney test. Each data point = one mouse.

(C) Gene expression of the PTN receptor *PTPRZ1* in DIPG primary tissue and cultures from published RNA-seq datasets and the present RNA-seq data from SU-DIPG-XIII (Grasso et al., 2015; Nagaraja et al., 2017). RNA-seq of the primary tissue was performed with one replicate. RNA-seq of the cell cultures were performed with two replicates.

(D) Exposure of DIPG cells to shRNA lentivirus targeting *PTPRZ1* achieved effective knock down of *PTPRZ1* gene expression as measured by qPCR, and of PTPRZ protein levels as measured by western blot, compared to a scrambled shRNA control or no shRNA exposure. qPCR experiments performed with n = 3 wells of cells and analyzed by one-way ANOVA with Tukey post hoc adjustment for multiple comparisons.

(E) Knock down of the PTN receptor *PTPRZ1* in SU-DIPG-XIII FL cells resulted in a decrease in baseline DIPG invasion toward unconditioned hNPC medium. n = 3 replicates/wells in SU-DIPG-XIII FL cells expressing *PTPRZ1* or scrambled shRNA and analyzed by unpaired, two-tailed Student's t test.

(F) DIPG cells with knock down of *PTPRZ1* had a mild decrease in cell viability by the CellTiter-Glo assay compared to a scrambled control or no shRNA exposure. Cell viability was measured in base medium without growth factors. n = 4 replicates/wells in SU-DIPG-XIII FL cells expressing *PTPRZ1*, scrambled, or no shRNA and analyzed by one-way ANOVA with Tukey post hoc adjustment for multiple comparisons.

(G) Knock down of *PTPRZ1* partially abrogates DIPG invasion toward SVZ hNPC CM or the PTN complex, compared to a scrambled control. n = 3 replicates/wells in SU-DIPG-XIII FL cells expressing *PTPRZ1* or scrambled shRNA and analyzed by unpaired, two-tailed Student's t tests for comparison between *PTPRZ1* knock down cells or scrambled shRNA control cells.

(H and I) DIPG cells with knock down of *PTPRZ1* exhibited 10-fold decreased total tumor size at two weeks following orthotopic xenografting, indicating decreased engraftment (H), but similar xenograft growth over time compared to scrambled shRNA control cells (I).

(J) Fewer DIPG cells with knock down of *PTPRZ1* invaded the SVZ when orthotopically xenografted into mice, compared to scrambled shRNA control cells.

In vivo experiments were performed with n = 8 mice per group. Bioluminescent flux measurements were analyzed by unpaired, two-tailed Mann-Whitney test for engraftment (H) or unpaired, two-tailed Student's t test for growth (I). Stereological cell counts at 8 weeks following xenograft were analyzed by unpaired, two-tailed Mann-Whitney test (J). Each data point = one mouse.

Data shown as mean ± SEM. *$p < 0.05$, **$p < 0.01$, ***$p < 0.001$.

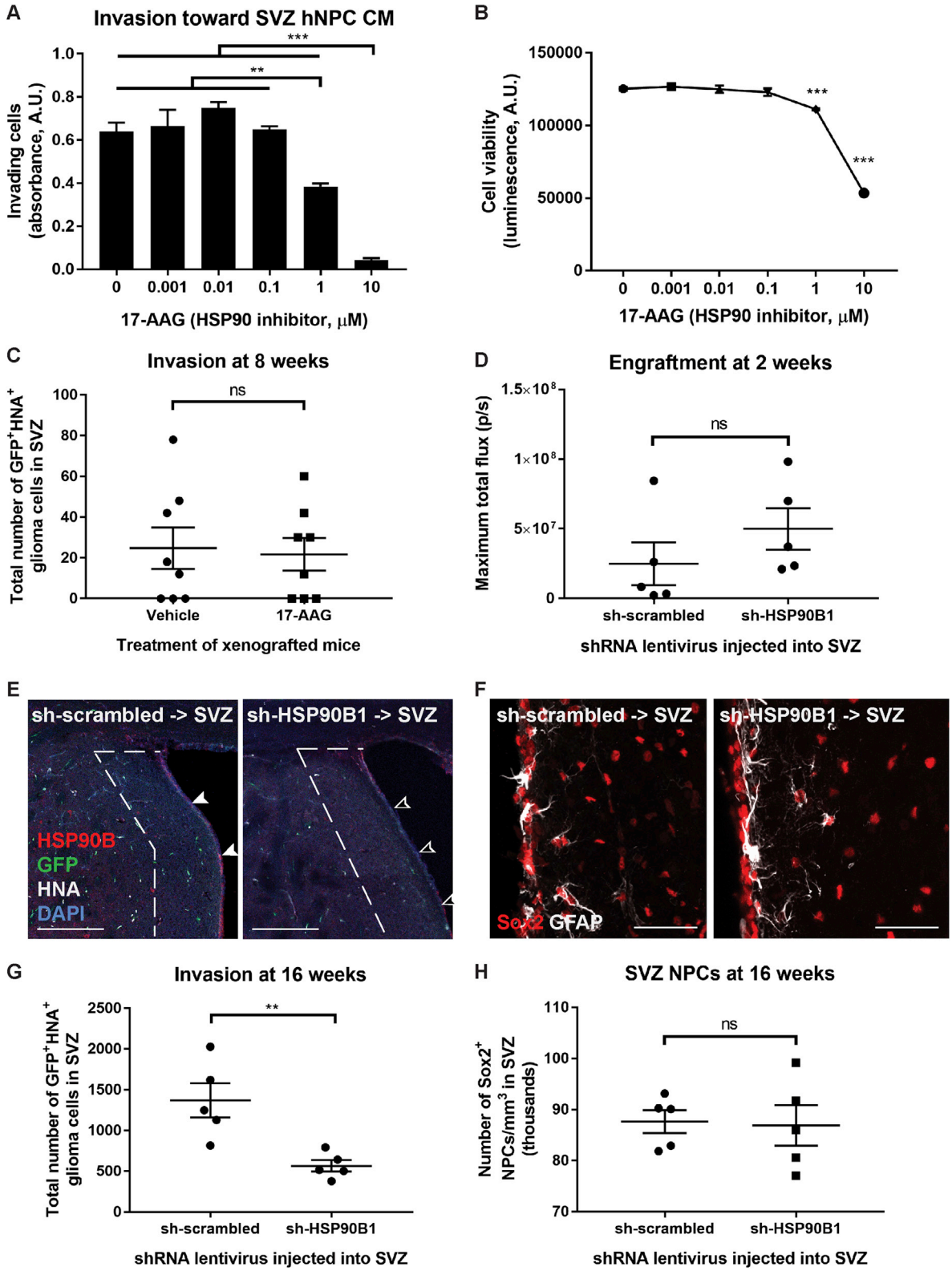

Figure S6. Inhibition of HSP90 by Drug and shRNA Lentivirus, Related to Figure 6

(A) Treatment of DIPG cells with an HSP90 inhibitor, 17-AAG, resulted in decreased invasion toward SVZ hNPC CM at high doses.

(B) Cell viability of DIPG cells treated with increasing doses of 17-AAG, by the CellTiter-Glo assay.

(legend continued on next page)

In vitro experiments performed with n = 3 replicates/wells (A) or n = 4 replicates/wells (B) in SU-DIPG-XIII FL cells and analyzed by one-way ANOVA with Tukey post hoc adjustment for multiple comparisons.

(C) Orthotopically xenografted mice that were treated with 17-AAG exhibited no difference in the number of DIPG cells invading the SVZ compared to a vehicle treatment control. In vivo experiments were performed with n = 8 mice per group. Stereological cell counts at 8 weeks following xenograft were analyzed by unpaired, two-tailed Student's t test. Each data point = one mouse.

(D) Tumor engraftment was equivalent in mice that received injections of shRNA lentivirus targeting *Hsp90b1* into the SVZ, compared to a scrambled shRNA control.

(E and G) Fewer orthotopically xenografted GFP^+ HNA^+ SU-DIPG-XIII FL cells invaded the SVZ, defined as a 200 μm-wide region adjacent to the lateral ventricles (outlined in dashed white lines), when sh-*Hsp90b1* lentivirus (right), compared to a scrambled shRNA control (left), was injected into the SVZ. White filled arrowheads denote areas of strong HSP90B expression in the SVZ (left); open arrowheads denote similar regions with low HSP90B expression after knock down (right). Scale bar, 200 μm. Control data are from the same mice as in Figures 6C–6F; these knock down experiments were run in parallel with a common control.

(F and H) The density of $Sox2^+$ NPCs in the SVZ was equivalent in mice injected with lentivirus expressing sh-*Hsp90b1* (right) or scrambled shRNA control (left). Scale bar, 50 μm. Control data are from the same mice as in Figures 6C–6F; these knock down experiments were run in parallel with a common control.

In vivo experiments (D–H) were performed with n = 5 mice per group. Bioluminescent flux measurements were analyzed by unpaired, two-tailed Mann-Whitney test (D). Stereological cell counts at 16 weeks following xenograft were analyzed by unpaired, two-tailed Student's t test. Each data point = one mouse (G and H). Data shown as mean ± SEM. $^{**}p < 0.01$, $^{***}p < 0.001$.

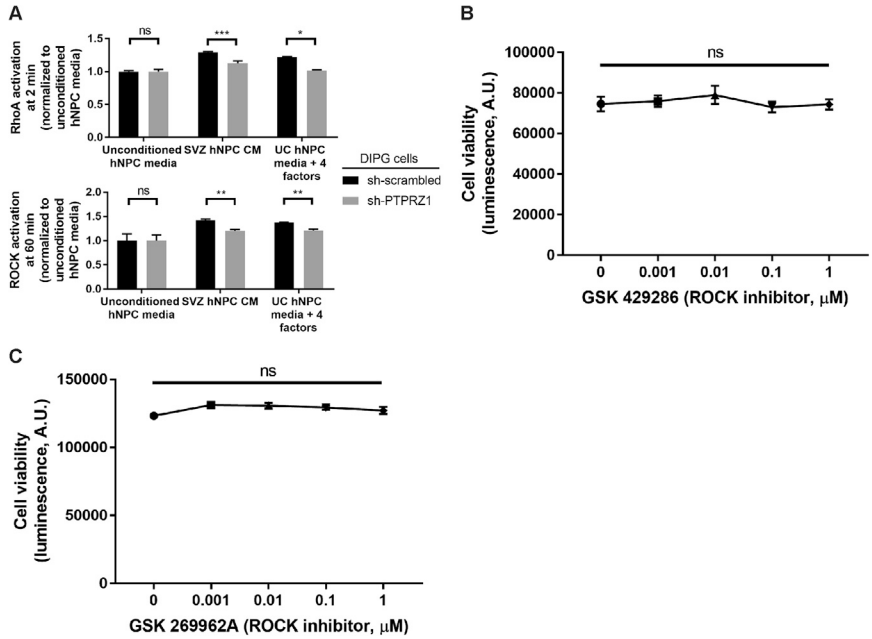

Figure S7. Rho/ROCK Activation and ROCK Inhibition in DIPG Cells, Related to Figure 7

(A) shRNA-mediated knock down of *PTPRZ1* in DIPG cells resulted in decreased activation of RhoA and ROCK upon exposure of DIPG cells to SVZ hNPC CM or to the PTN complex, compared to a scrambled shRNA control. n = 3 replicates/wells in SU-DIPG-XIII FL cells expressing *PTPRZ1* or scrambled shRNA and analyzed by unpaired, two-tailed Student's t tests for comparison between *PTPRZ1* knock down cells or scrambled shRNA control cells.

(B and C) Treatment of DIPG cells with two ROCK inhibitors: GSK 429286 (B) or GSK 269962A (C) do not affect cell viability at sub-μM concentrations. All experiments performed with n = 4 replicates/wells in SU-DIPG-XIII FL cells and analyzed by one-way ANOVA with Tukey post hoc adjustment for multiple comparisons.

Data shown as mean ± SEM. *$p < 0.05$, **$p < 0.01$, ***$p < 0.001$.